Estimating paleobathymetry with quantified uncertainties: a workflow illustrated with South Atlantic data

L. Pérez-Díaz[1*] & G. Eagles[2]

[1] *Royal Holloway University of London, TW20 0EX, Egham, Surrey, UK.*

[2] *Alfred Wegener Institute, Helmholtz Centre for Polar and Marine Research, Am Alten Hafen 26, 27568, Bremerhaven, Germany.*

**Corresponding author (email: lucia.perezdiaz@rhul.ac.uk)*

Abstract

We present and illustrate a workflow to produce paleobathymetric reconstructions, using examples from the South Atlantic ocean. With a recent high-resolution plate kinematic model as the starting point, we calculate an idealised basement surface by applying plate-cooling theory to seafloor ages and integrating the results with depths along the extended continental margins. Then, we refine the depths of this basement surface to account for the effects of sedimentation, variations in crustal thickness and dynamic topography. Finally, the corrected idealised surface is cut along appropriate plate outlines for the desired time slice and reconstructed using appropriate Euler parameters.

In order to assess the applicability of modelled results, we critically examine the limitations and uncertainties resulting from the datasets used and assumptions made. Paleobathymetry modelled with our approach is likely to be least reliable over parts of large igneous provinces close to the times of their eruption, and most reliable within the oceanic interiors for Neogene time slices. The uncertainty range is not smaller than 500 m for any significant region at any time, and its mean over 95% of locations in all time slices is close to 1800 m.

Paleobathymetry is an essential boundary condition for studies and models of paleocirculation, paleoclimate and hydrocarbon prospectivity. By integrating published studies about plate kinematics and the thermal structure of oceanic lithosphere with subsidence models for continent-ocean transition zones, grids of sedimentary and crustal thickness, and dynamic topography estimates, we have produced a workflow that can be used for any oceanic basin for which tectonic motions are well constrained. Here, we describe this workflow using the South Atlantic (Fig. 1) as an example.

At first order, plate tectonics controls paleobathymetry both by determining the changes in the geographical location of the lithosphere and the changes in its vertical level (through the mechanism of thermal subsidence). Using a kinematic model of South Atlantic opening (Pérez-Díaz & Eagles, 2014) as the starting point, we model paleobathymetry following the steps below:

(1) We use a high-resolution seafloor age grid (Pérez-Díaz and Eagles, 2017), derived from the plate kinematic model, to model the subsidence of oceanic lithosphere as a function of its age by applying plate cooling theory (GDH1; Stein & Stein, 1992).

(2) We implement a method for modelling the subsidence of Continent-Ocean Transition Zones (COTZs) through time, which allows us to extend the thermally subsiding surface as far as areas of unstretched continental crust at the ocean margins.

(3) We refine the resulting top-of-basement surface to account for other factors affecting bathymetry at smaller scales or amplitudes, both within the ocean and the COTZs (variations in sediment and crustal thickness; topography of Large Igneous Provinces (LIPs), aseismic ridges and seamounts and dynamic topography).

Some steps within this workflow account for processes that are relatively well understood and/or they use data sets whose uncertainties are well known, such as the age grid and its application in calculating oceanic thermal subsidence. Others are more susceptible to introduce errors due to large inherent uncertainties in data sets (e.g. dynamic topography) or poor knowledge or understanding of the timing or identity of processes (e.g. in COTZ subsidence). We describe these uncertainties and a method for quantifying them that allows us to present deepest and shallowest paleobathymetric error models for any given model age.

Generating top-of-basement surfaces

Thermal subsidence

The thermal evolution of oceanic lithosphere through time is one of the most frequently-revisited problems in geodynamics. Observations of the decrease in heat flow and increase in depth with seafloor age have prompted two main groups of models aiming to describe the way in which the oceanic lithosphere cools and subsides as it spreads away from mid-ocean ridges. In one, the lithosphere behaves as the cold upper boundary layer of a cooling half-space ("Half-space" models; e.g. Turcotte & Oxburgh, 1967; Parker & Oldenburg, 1973;

Davis & Lister, 1974). Comparison of model predictions to heat flow and depth data shows that half-space cooling models systematically overpredict depth and underpredict heat flow for older oceanic lithosphere, although small areas of seafloor following half-space subsidence trends can be found for almost all available ages of oceanic lithosphere (e.g. Adam & Vidal, 2010). The second group, of so-called plate-cooling models, results from a desire to portray the more widespread observation of seafloor flattening with age. They are built by fitting curves to observations of the variability of seafloor depth or heat flow with age, assuming that they characterise the cooling and thermal contraction of a lithosphere whose isothermal lower boundary flattens with age (Langseth *et al.*, 1966: McKenzie, 1967). This flattening has been variously attributed to shear heating in the asthenosphere (Schubert *et al.* 1976), radioactive heating (Forsyth, 1977; Jarvis & Peltier, 1980), dynamic phenomena (Schubert and Turcotte, 1972; Schubert *et al.* 1978; Morgan & Smith, 1992), and thermal rejuvenation by hotspot reheating events (Crough, 1978; Heestand & Crough, 1981; Nagihara *et al.* 1996; Smith, 1997) or smaller-scale convection in the uppermost mantle (Afonso et al., 2008). An in-depth review of these processes is provided by McNutt (1995), but here it is enough to note that attempts to improve thermal models by accounting explicitly for any of them have not produced significant improvements to predictive models for seafloor depth with age. With these considerations in mind, we have not attempted to generate a best-fitting depth-age curve for the South Atlantic, for which we find that plate-cooling models in general and GDH1 in particular (Stein & Stein, 1992) adequately depict thermal subsidence where the seafloor age is known (Figure 2). Other thermal models may be preferable for different ocean basins and should be given some consideration when modelling thermal subsidence.

For the present day, we use the seafloor age grid of Pérez-Díaz & Eagles (2017) directly as input to calculate depths below sea level due to thermal subsidence as modelled by GDH1 (Stein & Stein, 1992) after having adjusted the equations to account for a deeper average ridge depth in the South Atlantic than that in GDH1 (-2657 m).

For any given time before present day (t), we first generate a correction surface that, when subtracted from the present-day age grid adjusts its ages to eliminate those younger than t (Figure 3a). Then, we apply GDH1 (Stein & Stein, 1992) equations to calculate a thermal subsidence surface for time t (Figure 3b).

Continent-Ocean Transition Zones' (COTZs) depth through time

In order to achieve smooth palaeobathymetric reconstructions covering not only the oceanic parts of an ocean basin but also extending over the neighbouring extended continental crust, the shape through time of the COTZs needs to be modelled. To make this possible, we generate an idealised subsidence surface that crosses the COTZ, seamlessly covering the space between its oceanic and continental extremes according to the following scheme:

1. The extent of the COTZ along the South American and African margins is defined by two lines: (1) a control line on land, located within undoubtedly continental and

unstretched lithosphere ("outer line" or OL) and a control line beyond the distal edge of the extended continental margin (onwards "inner line" or IL), within undoubtedly oceanic crust. These lines are conservative estimates that we have digitised by taking into account the location of the inward and outward edges of the ensemble of Continent-Ocean Boundary (COB) identifications compiled by Eagles *et al.* (2015) as well as the locations of cratonic areas within South America and Africa.

2. Depths along the IL for time *t* are determined using GDH1 and the age grid (Stein & Stein, 1992; Pérez-Díaz and Eagles, 2017).
3. Heights along the OL are fixed for times between the onset of seafloor spreading and present day. These depths are sampled from a present-day topography map (Smith and Sandwell 1997) from which the isostatic contributions of variable sediment and crustal thickness to topography as well as those of dynamic topography have been removed.

With IL and OL depths for time *t* set, depth profiles between these two control lines might be modelled in a number of ways. At long wavelengths, COTZs can be treated as thermally subsiding or as flexural edge-of-plate or intraplate features. Figure 4 shows that simple flexural calculations produce in many cases theoretical bathymetric profiles across COTZs that, when the effects of sedimentation, stretching and dynamic topography are restored, closely resemble present-day observations. However, in some areas, a flexural curve does a poor job of replicating the shape of the margin. For this reason, we take an alternative approach that uses present-day bathymetry as a guide to the past shape of COTZs and is likely to be more applicable in ocean basins globally. We start by extracting depth information, at equally spaced points between IL and OL, from a map of present-day bathymetry corrected for the isostatic effects of sediment and crustal thickness variations and dynamic topography. By doing this, flowlines across COTZs become depth profiles independent of sedimentation and crustal stretching, whose effects vary with time. These depth profiles are then normalised and adjusted so that points along the IL always lie at depths predicted by GDH1 (Stein & Stein, 1992).

This approach implies assuming that long-wavelength depth profiles of COTZs only change in response to sedimentation, cooling of the oceanic lithosphere, and dynamic support from the convecting mantle, but that at isostatically-supported wavelengths the shape of the underlying basement is largely a consequence of extensional tectonics in the upper crust and breakup volcanism and therefore remains constant post-breakup. This assumption finds support in physical and numerical models of continental margin evolution (see for example Blaich *et al.* 2010; Huismans & Beaumont, 2011; Brune *et al.* 2014). Because currently we make no attempt to palinspastically restore the extended continental margins, the assumption of stable post-breakup basement topography should not introduce large errors.

Goswami *et al.* (2015) present a modelling method for reconstructing present-day global ocean bathymetry whose treatment of COTZs bears many similarities to the one we describe above. They calculate depth to basement at the seaward limit of COTZs by applying plate-cooling theory to oceanic lithosphere, using the age grids of Müller *et al.* (2008a). Then, they adjust these depths by accounting for an isostatically corrected sediment layer and generate

margin profiles by identifying, across COTZs, three segments (shelf, slope and rise) to which they apply distinct gradients calibrated from stacked global bathymetry curves across several of the world's oceans. By following this approach, they aim to account for the heterogeneity of extended continental margins. Although they follow a process-based approach and their results are shown to closely replicate modern bathymetry as portrayed by the ETOPO1 dataset (Amante & Eakins, 2009), they make no attempt at integrating the effects on depth of dynamic topography and variable oceanic crustal thickness and use a different seafloor age dataset than the one we use here (Pérez-Díaz & Eagles, 2017). Further to this, by using global bathymetry curves instead of present-day COTZ observations, their approach is more likely to smooth over local features.

Other contributors to bathymetry

In order to reduce uncertainty in palaeobathymetric reconstructions, the contributions to depth of second-order processes need to be quantified and used to correct the basement surfaces described in the previous section (Figure 5). An initial idea of the contribution of these processes to bathymetry can be obtained by subtracting the present-day modelled basement surface (Figure 5a) from a map of present-day bathymetry derived from satellite altimetry data. When this is done, a series of residual bathymetry anomalies are revealed (Figure 6). Positive anomalies (warm colours) arise when the seafloor is shallower than the modelled upper surface of the lithosphere. Sediment build-up and crustal thickening by volcanic/plutonic processes both give rise to positive anomalies. Negative anomalies (cold colours), such as those observed in the Argentine Basin, show a less localized character. They mark areas where the seafloor is deeper than predicted by the GDH1 model of a thermally subsiding lithospheric plate (Stein & Stein, 1992). The use of a different thermal model for oceanic lithosphere would yield different residual anomalies.

In steps, we adjust the present-day modelled top-of-basement surface (Figure 5a) to account for the depth effects of (1) sedimentation, (2) variable crustal thickness and (3) dynamic topography. The resulting further residual bathymetry anomalies, calculated by subtracting the top-of-basement surface adjusted for one or more of these processes from present-day satellite-derived bathymetry, are a useful context in which to interpret the uncertainties involved in the data used and the workflow itself. This is fundamental when applying the workflow to times before present day, in order to understand the limitations in palaeobathymetric reconstructions.

When referring to residual bathymetry anomalies (R), we will use a notation of the form $R_{x1\ldots3}$ with the set $x_{1\ldots3}$ consisting of one or more of the following: *s* (a correction for sediment thickness), *c* (a correction for crustal thickness) or *d* (a correction for dynamic topography). For example, R_{sd} are residual bathymetry anomalies after present-day dynamic topography and the isostatic effects of sediment thickness variations are corrected for. In other words, if we assume that we know sediment thickness and dynamic topography perfectly, then R_{sd} reveals the bathymetric signal of variations in crustal thickness alone.

Sedimentation

The density of sediment is greater than that of the water mass it replaces during sedimentation. Therefore, deposition of a sediment layer will cause the lithosphere to sink in response to the increased load. If the thickness of this sediment layer is known, the isostatic response of the lithosphere under it can be calculated. This isostatic correction (I) when applied to measured present-day bathymetry adjusts seafloor depth to account for a certain thickness of sediment (s) and its isostatic signal. We use Sykes (1996) approximation for the relationship between I and s and the sediment thickness map of Laske *et al.* (2013) for the South Atlantic (Figure 7a) to calculate the isostatic correction from sediment thickness, as follows:

$$I = 0.43422s - 0.010395s^2 \quad \text{Eq. 1}$$

Assuming the sediment thickness map used is a reliable representation of reality, by applying this isostatic correction to the map of predicted basement depths (Figure 5a), the effects of sedimentation are accounted for (Figure 7b), and the residual bathymetry anomalies can be reduced accordingly (Figure 7c).

For times in the past, it is necessary to undo the effects of sediment that had yet to be deposited. We calculate the sediment thickness from the present-day grids of Laske *et al.* (2013) by assuming a linear sedimentation rate.

Crustal thickness

In a crust of variable thickness, and assuming a value of average thickness which, for oceanic crust, will be something between 5 and 10 km (White *et al.* 1992), the lower density of the oceanic crust with respect to the underlying mantle that supports it means that areas thicker and thinner than average will give rise to positive and negative residual bathymetry anomalies. Accounting for the effects on bathymetry of variations in crustal thickness presents a greater challenge than doing so for variations in the thickness of the sediment cover. This is so because the best available crustal thickness grid (CRUST1.0, Laske *et al.* 2013) is of low resolution (1 degree, 111.2x111.2 km at the equator), and in most cases does not image seamounts or other regional volcanic constructs where the oceanic crust is thicker than its surroundings. The relationship between crustal thickness and the residual anomaly it gives rise to (assuming Airy isostasy) can be written as:

$$Y = C + R + M \quad \text{Eq. 2}$$

Here, Y, the total crustal thickness, equals the sum of C (average oceanic crust thickness), R (a residual bathymetry signal which could be R_{sd}, R_s, or R_d) and M (the depth of the crustal root below the base of the neighbouring average oceanic crust). Assuming Airy isostasy, a flat base of the crust, average oceanic crustal thickness of 7 km (which, for South Atlantic spreading rates is a reasonable value (White et al., 1992)), then ρ_c = 2950 kg/m^3, ρ_w = 1030 kg/m^3 and ρ_m = 3300 kg/m^3 and, rearranging:

$$R = \frac{(Y-7)}{6.4857} \quad \text{Eq. 3}$$

We quantify the depth effects of crustal thickness variability by applying this equation to the crustal thickness estimates from CRUST1.0 (Figure 8a, Laske *et al.* 2013). Modelled depths, already accounting for the effect of sediment load (Figure 7b), can subsequently be further adjusted to also account for the footprint of variations in crustal thickness (Figure 8b). As a result, positive residual anomalies are reduced significantly along the extended continental margins (Figure 8c). However, because CRUST1.0 fails to clearly image large areas of hotspot-related crustal thickening within the oceanic interiors, many strong local positive anomalies remain (e.g. Rio Grande and Walvis Ridges, Agulhas Rise, Shona Rise, Meteor Rise, Islas Orcadas Rise, NE Georgia Rise, Cameroon Volcanic Line).

For times in the past we apply the crust correction to all time steps to compensate for instantaneous stretching that affected the COTZs prior to the onset of spreading modelled by Pérez-Díaz & Eagles (2014). A further step, necessary to account for post-breakup topography built as a result of hotspot activity whose effects on crustal thickness are not captured in CRUST1.0, is described in a later section.

Dynamic topography

Viscous stresses transmitted vertically to the lithosphere from zones of contrasting buoyancy in the Earth's mantle are known to be responsible for its long wavelength uplift or subsidence. The surface expressions of these mantle fluctuations are generally referred to as dynamic topography (Pekeris, 1935; Morgan, 1965; McKenzie, 1977; Hager & O'Connell, 1981; Parsons & Daly, 1983; Richards & Hager, 1984; Hager *et al.* 1985).

Models of dynamic topography such as those developed by Bernhard Steinberger for Müller *et al.* (2008b) (Figure 9a) can be used to further reduce the residual bathymetry anomalies in figure 8c, as shown in Figure 9c. For times in the past, we account for the effects of dynamic topography by reconstructing plate positions into the mantle's absolute reference frame (Torsvik *et al.* 2008) and using Steinberger's dynamic topography reconstructions.

Using residual anomalies as a predictive tool

The differences between maps of modelled basement depths, such as that shown on figures 7b or 8b, accounting for the effects of any two of the three processes outlined above and present-day bathymetry can be used as a predictive tool for the effects of the third of the processes. Figure 8b accounts for variable sediment and crustal thicknesses, so the residual anomalies resulting from subtracting these depths from present-day bathymetry will provide insights into dynamic topography. In this section we model each of the three processes discussed by assuming that, once two of them have been accounted for, the remaining residual bathymetry anomalies are solely a result of the third of the processes. How close

predictions made in this way are to reality depend on how well the effect of the two processes from which the third is derived are known or modelled, as well as the uncertainties in GDH1 (Stein and Stein, 1992) and bathymetric data. This becomes evident in the next section, with sediment thickness predictions being strongly affected by the uncertainties in crustal thickness and dynamic topography grids.

Sediment thickness predictions

Sediment thickness (s) can be calculated substituting for I in Sykes' polynomial (Sykes, 1996), so that:

$$s = \frac{0.43422 \pm \sqrt{0.1885 - 0.04159(R_{cd})}}{0.02079} \quad \text{Eq. 4}$$

R_{cd} here are the residual bathymetry anomalies resulting from subtracting a modelled top-of-basement surface, accounting for dynamic topography and variations in crustal thickness, from present-day satellite-derived bathymetry.

Figure 10 shows the differences between the sediment thickness grid of Laske et al. (2013) and that modelled following the steps outlined above. If we ignore the very thick false sediment signals resulting from the residual bathymetry anomalies attributable to the Rio Grande-Walvis pair and other LIPs, sediment distribution is similar in both grids. The largest differences in sediment thickness appear along the margins, with modelled thickness being much larger and covering a greater area. Again, this may partly be a result of a crustal thickness grid that poorly images changes in crustal structure near the continents. The Argentine Basin looks fairly different in both grids, (compare area labelled "S2" in both panels of figure 10), which CRUST1.0 presents with nearly 5 km of sediment but the isostatic model suggest may be almost sediment free.

Crustal thickness predictions

Crustal thickness (Y) can be calculated from residual bathymetry anomalies (R_{sd}) by rearranging equation 2:

$$Y = 6.4857R_{sd} + 7 \quad \text{Eq. 5}$$

The residual bathymetry anomalies used here (R_{sd}) are the differences in depth between present-day bathymetry and a basement surface modified to account for sedimentation and dynamic topography. At first glance, the difference in resolution between CRUST1.0 (Laske et al., 2013) and the grid of predicted crustal thickness stands out (Fig. 11). Crustal thickness along the margins is similar in both grids, with the exception of the margin segment immediately north of Rio Grande Rise along the South American margin, where predicted crustal thicknesses are much larger than those shown by CRUST1.0 (C1 in figure 11).

Frustratingly few independent data exist to help assess the cause of this difference (Chulik et al., 2013). The Argentine basin represents an example of the opposite, an area where predicted crustal thickness is smaller than the seismic-derived estimate shown by CRUST1.0. In this particular region, when one looks at the sediment thickness grid (Laske et al., 2013) (Fig. 10a) the similarity between the shape of the area of thicker crust and that of thicker sediment cover is noticeable (C2 and S2 in figures 10a and 11a). It is possible that both sediment and crustal thickness really are greater in that part of the Argentine basin, in which case the lack of an accompanying gravity anomaly (e.g. Sandwell et al., 2014) would need careful explanation. A more plausible possibility is that either sediment or crustal thickness (or both) have been separately used as interpretations for a particular seismic signature, resulting in overestimated values here.

Large Igneous Provinces (LIPs), aseismic ridges and seamounts

CRUST1.0 (Laske *et al.* 2013) does not portray the expected or more-recently proved variations in crustal thickness associated with many LIPs, aseismic ridges and seamounts. Because these features are not direct consequences of thermal subsidence of the ocean they cannot be inferred from plate kinematic models. In order to include these features in reconstructions of palaeobathymetry, we therefore follow the steps below:

First, we compile a dataset of longitude-latitude-age points along hotspot tracks in the South Atlantic from published literature (O'Connor & Duncan, 1990; O'Connor *et al.* 2012; O'Connor & Jokat, 2015). This contains points along the Tristan, St. Helena, Bouvet, Martin Cas, Ascension, Gough, Discovery and Shona hotspot trails. Some of the ages are based on radiometric dating of drilled or dredged samples. Others are based on O'Connor & Duncan's (1990) modelling of plate motion over a set of fixed hotspots in the mantle.

Second, for a reconstruction at time *t* Ma, points in the dataset dated as younger than *t* are filtered out. Areas within a 250 km radius of the remaining points (whose ages are older than or equal to *t*) are used to extract values of R_{scd} residual bathymetry (figure 9c) that we can reasonably expect to relate to crustal thicknesses that exceed those shown in CRUST1.0. This radius is intended to reflect the effects of a wide plume head or sublithospheric flow of melt away from the plume conduit.

Finally, a low-pass filter is applied to the extracted residual signals to ensure that wavelengths between 250 and 100 km are progressively weakened and shorter wavelengths are cut out completely. The main aim in doing this is to smooth out any sharp edges at 250 km distance from the age-constrained points in the dataset being used. The result is a grid of excess topography with values that increase smoothly from 0 to the thickness shown by R_{scd} within the locus of grid cells that we might expect to have experienced crustal thickening as a result of hotspot activity by time *t*. These grids of excess topography related to hotspots are used as the fourth dataset to refine a thermally subsiding top-of basement surface (together with the sediment and crustal thickness and dynamic topography datasets reviewed earlier) to produce palaeobathymetric models (Figure 12).

Including LIPs is an important step in order to produce palaeobathymetric reconstructions for the purpose of paleoceanographic interpretation, because LIPs have the potential to form barriers to water circulation at multiple depths (e.g. Wright and Miller, 1996; Poore *et al.*, 2006; Ehlers and Jokat, 2013). The method we follow to include LIPs involves assuming that, when one removes from present day bathymetry the effects of sedimentation, crustal thickness variations and dynamic topography, the remaining residual bathymetry anomalies reflect the existence of volcanism-related excess topography. Therefore, predicted LIP topography may be either over or underestimated, depending on the inaccuracies of the sediment, crustal thickness and dynamic topography datasets.

Dynamic topography predictions

After accounting for the isostatic effects of crustal thickness variations and sedimentation and comparing R_{sc} to satellite-derived present-day bathymetry we filter the residual anomalies in order to extract signals whose wavelength is within the characteristic range for dynamic topography (Hoggard, White, and Al-Attar, 2016). In order to do this, we use a bandpass filter (2nd order Butterworth polynomial filter) that passes wavelengths of between 2000 and 3000 km and removes anomalies whose wavelength is shorter or longer than any of these cut-off values.

The result of doing this is shown together with the dynamic topography grid of Müller et al. (2008b) in figure 13. In terms of the distribution of positive and negative anomalies both grids are broadly comparable, with a strong negative anomaly in the Argentine Basin region and positive anomalies towards the African plate. However, and similarly to what happens with sediment thickness predictions from R_{cd}, the failure of CRUST1.0 to image many of the South Atlantic's aseismic ridges hinders the dynamic topography prediction. In this case, strong false positive dynamic topography is predicted in areas where aseismic ridges are located (Rio Grande-Walvis Ridges, Agulhas Rise and North East Georgia Rise are clear examples), as a result of a satellite-derived bathymetry which is much shallower than that depicted over an isostatically compensated cooling lithosphere (lacking any crustal thickening as a result of volcanism). At least some of the large apparent positive dynamic topography off the coast of southern Africa is therefore likely to result from a combination of underestimated sediment thickness in the Cape Basin and underestimated crustal thickness, with features such as the Walvis Ridge, Meteor Rise and Shona and Discovery seamounts unaccounted for by CRUST1.0 (Laske et al., 2013).

Quantification of total uncertainty in palaeobathymetric grid models

As described above, our paleobathymetric estimates are generated by calculating the depth to the top surface of a lithosphere that forms by conductive cooling of the mantle, and then adjusting this surface for the isostatic effects of varying thicknesses of the crust and sediments overlying it, and for the effects of vertical stresses transmitted to its base during

convection of the viscous mantle below. All of these considerations are affected by errors with various sources, whose effects are to produce an estimate of paleobathymetry that is either deeper or shallower than the unknown true value. We describe quantifications of these effects in the following section.

Uncertainties in calculations of thermal subsidence

Uncertainty in the depth to the top surface of the thermally subsided lithosphere step might be dominated by the choice of lithospheric thermal model or the uncertainties in the chosen model itself. The standard deviations of seafloor depths over same-aged areas in the South Atlantic show that so-called plate cooling models are to be preferred over half-space models for predicting seafloor depth, but are less prescriptive of any particular plate cooling variant. We chose to use the GDH1 model of Stein & Stein (1994) because of its closest resemblance to mean depths in the South Atlantic, which for most ages vary by less than 100 m from GDH1 predictions, and do not exceed 300 m for any age (Pérez-Díaz, 2016).

A more significant and readily-quantifiable estimate of the uncertainty in using GDH1 is that which propagates through it from uncertainty in the seafloor age. Pérez-Díaz and Eagles (2017) provided their age grid with an accompanying set of quantified age uncertainties, which they showed to imply variable but potentially large (600 m) long-wavelength errors in paleobathymetry near mid-ocean ridges acting during the Cretaceous normal polarity superchron, but smaller errors in other settings. The age uncertainty is unsigned, meaning these errors might have the effect of producing inappropriately shallow or inappropriately deep estimates of paleobathymetry.

We extended the thermally-subsided surface across the model COTZs simply by stretching the present-day basement surface between an undoubtedly-oceanic inner line and an outer line on supposedly non-extended continental crust to fit the contemporary range between the thermally-subsided depth of the inner line and the present-day height of the outer line in the absence of dynamic topography. To this, we apply an estimate of uncertainty appropriate for subsidence by thermal contraction using the relationships derived assuming one-dimensional heat conduction by McKenzie (1978). The potential depth error we calculate in this instance propagates from an assumed error in the age of instantaneous rifting in those relationships. In our paleobathymetric modelling process, this age is implicitly the same as the age of the COTZ's IL. In the uncertainty analysis, this serves as a minimum age estimate for the end of rifting in the COTZ because of the choice of an IL that is undoubtedly oceanic and therefore definitively post rifting. The effect of this age being inappropriately young is to produce COTZ model depths at any time that are inappropriately shallow. For our analysis, we apply a potential error of 10 Myr towards older ages for the end of instantaneous rifting at the outer line that varies smoothly to the value of the oceanic age grid error at the inner line. The depth uncertainty that this produces is largest close to the IL and for times close to the age of the IL.

We have not attempted to quantify other processes (e.g. flexure; gravity gliding) that are known to affect short wavelength bathymetry in specific shelf and slope settings at the present day.

Uncertainty in crustal thickness estimates

The largest uncertainties related to variations of crustal thickness are the result of the dataset's low spatial resolution (Laske *et al.* 2013), which shows very little variation in oceanic crustal thickness. Compared to this, the natural variation of normal oceanic crustal thickness formed at plate divergence rates like those encountered in the South Atlantic is thought to occur within a tight, but nevertheless significant, range (4-8 km, mode near 7 km) as a consequence of the crust's formation by adiabatic compression of well-mixed upper mantle rocks (White et al., 1992). A more recent study has shown that this variation is partially age dependent, and suggested a gradual cooling-related reduction in mantle fecundity as its cause (van Avendonk et al., 2017). To account for possible effects of erroneous oceanic crustal thickness, we allowed the 7 km steady-state crustal thickness in equation 3 to vary with age according to van Avendonk et al.'s (2017) regression, and permitted its subject to then vary by a further ±1.0 km, which captures nearly 100% of the remaining present-day off-axis variability in measured oceanic crustal thicknesses in van Avendonk et al.'s (2017) compendium. Crustal thickness can vary from the gridded values in such a way that the paleobathymetry produced using it is either inappropriately shallow (where the true thickness is at its maximum above the gridded thickness and the long-term average is at its minimum) or inappropriately deep (where the true thickness is at a minimum below the gridded thickness and the long-term average is at its maximum). Given these possibilities, we produce both deepening and shallowing error surfaces for crustal thickness uncertainties.

Laske et al's (2013) crustal thickness grid also fails to show the thicker igneous crust underlying many unstudied or less-studied oceanic large igneous provinces, resulting in large areas of erroneously deep paleobathymetry. Our modelling procedure accounts for this inadequacy by isolating the paleo-residual topography along known hotspot tracks and restoring it to the reconstruction. The residual bathymetry used is derived from present-day bathymetry, whose uncertainty might be in the range of 200 m (Smith and Sandwell, 1997). A larger error is entailed in the assumption that the large igneous provinces at the present-day are preserved products of magmatic-volcanic events dating from the instants of plume arrival beneath the lithospheric regions they are built on. This assumption is inadequate, as shown by the widespread determination of late-stage volcanism on submarine large igneous provinces or the dated variability of lava ages exposed on Iceland, which suggests the large igneous province there built up over the last 20 Myr. Based on this, sets of our paleobathymetric maps may be too shallow around active hotspots over 20 Myr-long periods. To capture some of the uncertainty coming from this expectation, and in the absence of robust estimates of the rate of large igneous province growth, we calculate a linear proportion of the residual bathymetry that varies between zero (20 Myr downstream of the hotspot), and 0.5 (at the hotspot location).

454

455 *Uncertainty in sediment calculations*

456 A further step to producing paleobathymetry is to load the thermally-subsided lithosphere
457 with a pile of sediments whose thicknesses are estimated on the basis of a global compilation
458 and as a linear proportion of the time elapsed between the time of the reconstruction and the
459 age of the crust. The effect of this loading is calculated using an empirically-derived isostatic
460 correction (Sykes, 1996). This correction uses densities derived mostly from seismic velocity
461 analysis and which follow a depth dependent trend, and represents an improvement over
462 others that forwardly assign a uniform density to the entire sediment package, resulting in
463 overestimated corrections (Sclater *et al.* 1977; Sclater *et al.* 1985; Hayes, 1988; Renkin &
464 Sclater, 1988; Kane & Hayes, 1992). Nonetheless, for sediment loads like the majority of
465 those shown in figure 7a, the various isostatic corrections yield similar results, and so the
466 uncertainties associated with the choice of isostatic correction scheme are not quantified here.

467 The global sediment thickness grid used (Laske *et al.* 2013) is based on large regional
468 compilations of sediment thickness contours derived from reflection and refraction seismic
469 velocity studies (Hayes, 1991). Because in many cases seismic basement is not imaged and in
470 those cases in which it is it may not represent the upper surface of the crystalline crust, the
471 sediment thickness shown by Laske *et al.* (2013) is a minimum estimate. To illustrate this, a
472 recent correlation of industry seismic datasets to global grids suggests a tendency for Laske et
473 al. (2013) to systematically underestimate sediment thickness by as much as 20% (Hoggard et
474 al., 2017), albeit within broad scatter. In contrast, Whittaker et al. (2013) suggested that the
475 effect of uncertainty in velocity solutions for sediment thickness estimates off southern
476 Australia may be in the region of 25% of the minimum estimated thickness. With this in
477 mind, for each time slice, we calculated the effect of a 25% increase in sediment load
478 throughout the study area. This effect decreases with age, because as part of our modelling
479 process the uncertainty in isostatic correction to basement depth is calculated using ever-
480 smaller proportions of the possible error in present-day sediment thickness.

481 A potentially large remaining uncertainty is related to the assumption, when reconstructing
482 sediment thickness for times in the past, of a linear sedimentation rate. This is a
483 simplification whose effect can be removed by a more appropriate approach for regions
484 where chronostratigraphic stage-scale isopach data sets exist. For now, in the absence of such
485 data for most parts of the South Atlantic, we do not quantify the assumption's effects on
486 paleobathymetry for the uncertainty analysis.

487

488 *Uncertainty in dynamic topography models*

489 The effects of global mantle circulation on topography are modelled with inputs from mantle
490 tomography and assumptions about the mantle viscosity profile (Müller *et al.* 2008b).
491 Variations in S-wave velocity obtained with seismic tomography are used to make
492 interpretations of the temperature and density heterogeneities within the mantle. Lateral

variations of density cause convective flow and provide insights about the locations of dynamic topography highs and lows. The amplitudes of these depend heavily on the mantle viscosity profile, and so assumptions about this parameter have a strong effect on dynamic topography models. An overview of the errors that ought to be expected from viscosity profiles derived from geoid fits is given by Panasyuk & Hager (2000).

For the present day, when misfits with respect to residual bathymetry anomalies are calculated, dynamic topography predictions from geodynamic models are generally found to be too high (Lithgow-Bertelloni & Silver, 1998; Panasyuk & Hager, 2000; Pari & Peltier, 2000; Cadek & Fleitout, 2003; Steinberger & Holme, 2008; Hager et al., 2016).

The grids of dynamic topography we use (Müller *et al.* 2008b) were tuned to portray dynamic topography within a ±1.5 km amplitude range. They use seismic tomography to infer density heterogeneities within a stratified mantle and account for the effects of latent heat release across the phase boundary at 660 km depth. Uncertainties in these models are largest for times in the past, with no dynamic topography estimates for times before 100 Ma and estimates for ages older than 70 Ma considered unlikely to be meaningful (Steinberger, pers. comm.). A further source of error lies in the fact that the modelled dynamic topography depends on modelled mantle convection that responds to tractions calculated using a global plate kinematic model whose South Atlantic plate motions are different from those we use for our paleobathymetries. The differences, in particular to the nature of the plate boundaries implied by those motions, however, are of small significance at the global scale, and the effects of the tractions are known to be of second order significance even for the pattern of whole mantle circulation (Steinberger et al., 2004).

The possible errors owing to dynamic topography in the modelling can be either positive (too much dynamic topography has been estimated and removed) or negative (too little estimated and removed). To quantify these, we compared Müller et al.'s (2008) estimate of present-day dynamic topography to our own estimate of present-day South Atlantic residual topography, which ideally at long wavelengths should be equivalent surfaces. We apply two standard deviations of the differences between these data sets (±288 m) as a plausible maximum error range at 0 Ma. By 70 Ma and later, we assume that dynamic topography is essentially unknowable, and thus apply a larger maximum range equal to two standard deviations of the entire variation for that time slice. For times between 0 Ma and 70 Ma, we apply a linear increase between the standard deviations used for those two ages.

Quantification of total uncertainty in palaeobathymetric grid models

Table 2 summarises the error considerations described above and classifies them according to whether they imply the calculated paleobathymetry to be too deep, or too shallow. By summation of each of these two uncertainty classes it is possible to produce (i) a maximum likely deepening correction and (ii) a maximum likely shallowing correction. Figure 14 shows examples of these corrections appropriate to modelled paleobathymetry at 60 Ma.

The maximum error range (the sum of the magnitudes of the shallowing and deepening components) implied in Figure 14 is 4908 m, which like all of the largest range values is encountered over parts of LIPs that are modelled to have been forming close to mid-ocean ridge crests at 60 Ma. This reflects our method's insensitivity to what we have assumed to be finite emplacement periods for those LIPs. This source of uncertainty dominates the upper end of the uncertainty ranges for all model ages, and should also be considered to dominate critical uncertainty in the precise timing of the production and removal of barriers and filters for paleo-abyssal currents.

The mean and standard deviation of the range shown in Figure 14, however, are 1317 m and 231 m, reflecting the more modest uncertainty ranges (minimum 794 m) calculated over the large areas of abyssal plain with thin sediment cover and monotonous oceanic crustal thickness. For Neogene time slices, in which the proportion of such material is larger owing to widening of the ocean, the mean of the uncertainty range reduces to less than 1100 m and the standard deviation to 200 m. In older time slices, the opposite is the case, with uncertainty in the time of instantaneous rifting in the COTZs becoming more significant, leading the mean of the uncertainty range at 110 Ma, for example, to approach 2300 m and its standard deviation 600 m.

Overall, these considerations are consistent with the expectation that confidence in our older time slices should be considered to be less than in our younger ones. Analysis of the full set of uncertainty ranges for all modelled ages suggests a confidence range of 1800 m (mean and two standard deviations) may be appropriate and conservative for 95% of nodes. This range, however, is not symmetrical about our paleobathymetric estimates because of the large range estimates over LIPs, which all imply the modelled paleobathymetry to be too shallow, and because of the asymmetry of the GDH1 and McKenzie (1978) age-depth curves for oceanic lithosphere and instantaneously-stretched COTZs. Given this, to best portray uncertainty, we sum our shallowing and deepening corrections with the modelled paleobathymetry to produce shallowest and deepest plausible bathymetries within uncertainties.

Assessment of uncertainty appropriateness

Figure 15 compares a present-day bathymetry and its shallowest and deepest uncertainty surfaces that have been generated using the procedures described above to the present-day bathymetry in the GEBCO 2014 grid (version 20150318, www.gebco.net), which is based on a combination of sparse ship soundings and interpolations based on satellite gravimetry. In view of the fact that our procedure is not designed to model short wavelength variations, the bottom part of the figure maps only those areas exceeding 50 km in diameter within which the GEBCO bathymetry completely lies outside the range implied by the shallowing and deepening uncertainties for their modelled counterparts. These areas amount to 5.6% of the modelled region, suggesting that, in terms of coverage at least, the volumes between our shallowest and deepest surfaces might well be considered as similar to 95% confidence estimates for the modelled paleobathymetric surfaces.

The distribution of nodes that lie deeper in the GEBCO 2014 estimates than their modelled counterparts has a mean of 211 m and a standard deviation of 245 m. The majority of these areas coincide with estimates of thick crust and/or thick sediments in CRUST1.0, in particular in the outer Argentine basin where large disagreements with the crustal and sediment thickness predictions of residual bathymetry have already been noted (Figure 10 and 11). In the Cape Basin, a smaller area of deeper-than-modelled seafloor may hint at a local lithospheric cooling history that differs from GDH1. The distribution of GEBCO 2014 nodes lying shallower than our shallowest uncertainty estimates is more skewed to large values: a mean of 1106 m and standard deviation of 597 m. The locations of these mismatches are centred on R_{csd} highs that have been incompletely sampled by our procedure for isolating and restoring LIP topography. Given their size and their concentration around the central Atlantic gateway, to whose evolution Albian and Cenomanian paleoclimate is likely to have been sensitive, future work may be necessary to more fully represent these areas and/or their uncertainties in paleobathymetry for those times.

Summary

To aid our summary, figure 16 shows South Atlantic paleobathymetry for a Paleocene time slice, modelled following the workflow described in this paper. This, and other time slices for the South Atlantic are presented, interpreted and discussed in geological and paleoceanographical terms by Pérez-Díaz and Eagles (Scientific Reports, in review). At this time, the topography of the mid-ocean ridge lies at depths close to 2600 m, as is the case for its present-day counterpart. Away from the ridge crest, the seafloor gradually drops down to depths in the region of 5700 m in four distinct basins (Brazil, Angola, Argentine and Cape Basins). These variations reflect our use of plate cooling theory to model thermal subsidence of the oceanic lithosphere from a high-resolution grid of seafloor ages derived from the kinematic model of Pérez-Díaz and Eagles (2014). Between and within these basins, rising up to several thousand metres above the modelled abyssal plains, a number of regional plateaus represent the forerunners of large igneous provinces like today's Rio Grande Rise and Walvis Ridge, which we have modelled as the products of intraplate volcanism related to hotspots over which the African and South American plates slowly moved. The deep ocean regions rise smoothly up towards continental shelves that rim the African and South American continents that lie much closer together than they do today. This variation reflects our application of isostatic corrections to model the bathymetric effects of large-scale sedimentation and changing crustal thickness at and across the extended margins of continents that have moved into their present relative positions as parts of two large lithospheric plates since early Cretaceous times. At very long wavelengths, modest and smooth deflections from the bathymetry predicted by these processes depict the effects of regional up- and downwarping of the lithosphere by slow convection of the viscous mantle rocks beneath the South Atlantic ocean. By forward considerations and by comparison to published point estimates of paleobathymetry at drill core sites, we show that the depths in this grid or grids like it for other time slices can conservatively be considered as accurate to within as little as 700 m over large oceanic parts of the map area, but much less so over short

distances near large igneous provinces and in early time slices. This accuracy approaches the vertical resolution of the model deep ocean in general circulation models, demonstrating that paleobathymetric maps built using it are suitable for use in deep-time paleoceanographic studies. Finally, our approach, being largely process- rather than data-based, can be expected to yield results of similar high confidence and quality for large areas of the world's paleo-oceans.

Acknowledgements

Both authors are grateful to Royal Holloway University of London and the Alfred Wegener Institute, Helmholtz Centre for Polar and Marine Research for funding. LPD would like to thank the COMPASS Consortium for further funding support.

References

Adam, C and V Vidal (2010). "Mantle Flow Drives the Subsidence of Oceanic Plates". In: Science 328, pp. 83–85. doi: doi10.1126/science.1185906.

Afonso, J.C., Zlotnik, S., Fernàndez, M., 2008. Effects of compositional and rheological stratifications on small-scale convection under the oceans: Implications for the thickness of oceanic lithosphere and seafloor flattening. Geophys. Res. Lett. 35, L20308. doi:10.1029/2008GL035419

Amante, C. and B. Eakins (2009). "ETOPO 1 Arc-minute global relief model: Procedures, data sources and analysis". In: NOAA Tech. Memo. NESDIS NGDC-24. Natl. Geophys. Data Center: Boulder, Colorado, p. 19.

Blaich, O. et al. (2010). "Structural architecture and nature of the continent-ocean transitional domain at the Camamu and Almada Basins (NE Brazil) within a conjugate margin setting". In: Petroleum Geology Conference Series 7, pp. 867–883. doi: 10.1144/0070867.

Brune, S. et al. (2014). "Rift migration explains continental margin asymmetry and crustal hyper-extension." In: Nature Communications 5(4014), pp. 1–9. doi:10.1038/ncomms5014.

Cadek, O and L Fleitout (2003). "Effect of lateral viscosity variations in the top 300 km on the geoid and dynamic topography". In: Geophysical Journal International 152, pp. 566–580.

Chulick, G.S., Detweiler, S. and Mooney, W.D. (2013). Seismic structure of the crust and uppermost mantle of South America and surrounding oceanic basins. Journal of South American Earth Sciences, 42, pp.260-276.

Crosby, A. G., D. McKenzie, and J. G. Sclater (2006). "The relationship between depth, age and gravity in the oceans". In: Geophysical Journal International 166(2), pp. 553–573. doi: 10.1111/j.1365-246X.2006.03015.x.

Crough, S. (1978). "Thermal origin of midplate hotspot swells". In: Geophysical Journal International 55(2), pp. 451–469.

Davis, E. and C. Lister (1974). "Fundamentals of ridge crest topography". In: Earth and Planetary Science Letters 21, pp. 405–413.

Doin, M. and L. Fleitout (1996). "Thermal evolution of the oceanic lithosphere: an alternative view". In: Earth and Planetary Science Letters 142, pp. 121–136. doi: 10.1016/0012-821X(96)00082-9.

Eagles, G., L. Pérez-Diaz, and N. Scarselli (2015). "Getting over Continent Ocean boundaries". In: Earth Science Reviews 151, pp. 244–265. doi:10. 1016/j.earscirev.2015.10.009.

Ehlers, BM. and Jokat, W. (2013). Paleobathymetry of the northern North Atlantic and consequences for the opening of the Fram Strait. In: Marine Geophys. Res. 34: 25. doi:10.1007/s11001-013-9165-9

Forsyth, D.W. (1977). "The evolution of the upper mantle beneath mid-ocean ridges". In: Tectonophysics 38(1-2), pp. 89–118. doi: 10.1016/0040-1951(77)90202-5.

Goswami, A. et al. (2015). "OESbathy version 1.0: A method for reconstructing ocean bathymetry with generalized continental shelf-slope-rise structures". In: Geoscientific Model Development 8(9), pp. 2735–2748. doi: 10.5194/gmd-8-2735-2015.

Hager, B. H. and R. J. O'Connell (1981). "A simple global model of plate dynamics and mantle convection". In: Journal of Geophysical Research 86(B6), pp. 4843–4867. doi: 10.1029/JB086iB06p04843.

Hager, B. H. et al. (1985). "Lower mantle heterogeniety, dynamic topography and the geoid". In: Nature 313(6003), pp. 541–545.

Hayes, D. E. (1991). "Marine Geological and Geophysical Atlas of the Circum-Antarctic to 30ºS". In: Antarctic Research Series, vol. 54, AGU. Washington DC.

Hayes, D. (1988). "Age-depth relationships and depth anomalies in the southeast Indian Ocean and South Atlantic Ocean". In: Journal of Geophysical Research 93(B4), pp. 2937–2954.

Heestand, R. and S. Crough (1981). "The effect of hot spots on the oceanic age-depth relation". In: Journal of Geophysical Research 86(1), pp. 6107–6114.

Hillier, J. K. and A. B.Watts (2005). "Relationship between depth and age in the North Pacific Ocean". In: Journal of Geophysical Research B: Solid Earth 110(2), pp. 1–22. doi: 10.1029/2004JB003406.

Hoggard, M. J., N. White, and D. Al-Attar (2016). "Global dynamic topography observations reveal limited influence of large-scale mantle flow". In: Nature Geoscience 9, pp. 1–8. doi: 10.1038/ngeo2709.

Hoggard M., J. Winterbourne, K. Czarnota, and N. White (2017), Oceanic Residual Depth Measurements, the Plate Cooling Model and Global Dynamic Topography, In: J. Geophys. Res., 122, doi:10.1002/2016JB013457.

Huismans, R. and C. Beaumont (2011). "Depth-dependent extension, two-stage breakup and cratonic underplating at rifted margins." In: Nature 473(7345), pp. 74–78. doi: 10.1038/nature09988.

691 Jarvis, G. and W. Peltier (1980). "Oceanic bathymetry profiles flattened by radiogenic
692 heating in a convecting mantle". In: Nature 285, pp. 649–651. doi:
693 10.1073/pnas.0703993104.

694 Kane, K. A. and D. E. Hayes (1992). "Long-Lived Mid-Ocean Ridge Segmentation". In:
695 Journal of Geophysical Research 97(92), pp. 317–330.

696 Langseth M. et al. (1966). "Crustal structure of the mid-ocean ridges". In: J. Geophys. Res.
697 71(22), pp. 341–352.

698 Laske, G. et al. (2013). "Update on CRUST1.0 - A 1-degree Global Model of Earth's Crust".
699 In: Geophys. Res. Abstracts 15(EGU2013), p. 2658.

700 Le Stunff, Y. and Y. Richard (1997). "Partial advection of equidensity surfaces: A solution
701 for the dynamic topography problem ?" In: Journal of Geophysical Research 102(B11), pp.
702 24655–24667.

703 Lithgow-Bertelloni, C. and P. Silver (1998). "Dynamic topography, plate driving forces and
704 the African superswell". In: Letters to Nature 395, pp. 345–348. doi: 10.1038/26212.

705 McKenzie, D. P. (1967). "Some remarks on heat flow and gravity anomalies". In: Journal of
706 Geophysical Research 72(24), pp. 6261–6273. DOI: 10 . 1029 / JZ072i024p06261.

707 McKenzie, D. (1977). "Surface deformation, gravity anomalies and convection". In:
708 Geophysical Journal of the Royal Astronomical Society 48(2), pp. 211–238.

709 McKenzie, D., (1978). "Some remarks on the development of sedimentary basins". In: Earth
710 and Planetary Science Letters, 40(1), pp.25-32.

711 McNutt, M. (1995). "Marine geodynamics: Depth-age revisited". In: Reviews of Geophysics
712 (Supplement), pp. 413–418.

713 Morgan, J. and W. Smith (1992). "Flattening of the sea-floor depth-age curve as a response to
714 asthenospheric flow". In: Nature 359, pp. 524–527.

715 Morgan, W. J. (1965). "Gravity anomalies and convection currents". In: Journal of
716 Geophysical Research 70(24).

717 Müller, R. D. et al. (2008a). "Age, spreading rates, and spreading asymmetry of the world's
718 ocean crust". In: Geochemistry, Geophysics, Geosystems 9(4). doi: 10.1029/2007GC001743.

719 Müller, R. D. et al. (2008b). "Long-term sea-level fluctuations driven by ocean basin
720 dynamics." In: Science 319, pp. 1357–1362. doi: 10.1126/science.1151540.

721 Nagihara, S., C. R. Lister, and J. G. Sclater (1996). "Reheating of old oceanic lithosphere:
722 Deductions from observations". In: Earth and Planetary Science Letters 139, pp. 91–104. doi:
723 10.1016/0012-821X(96)00010-6.

O'Connor, J. M. and R. A. Duncan (1990). "Evolution of the Walvis Ridge-Rio Grande Rise Hot Spot System: Implications for African and South American Plate motions over plumes". In: Journal of Geophysical Research 95(B11), pp. 17475–17502. doi: 10.1029/JB095iB11p17475.

O'Connor, J. M. andW. Jokat (2015). "Tracking the Tristan-Gough mantle plume using discrete chains of intraplate volcanic centers buried in theWalvis Ridge". In: Geology 43(8), pp. 715–718. doi: 10.1130/G36767.1.

O'Connor, J. M. et al. (2012). "Hotspot trails in the South Atlantic controlled by plume and plate tectonic processes". In: Nature Geoscience 5(10), pp. 735–738. doi: 10.1038/ngeo1583.

Panasyuk, S. V. and B. H. Hager (2000). "Inversion for mantle viscosity profiles constrained by dynamic topography and the geoid , and their estimated errors". In: Geophysical Journal International 143, pp. 821–836.

Pari, G. andW. R. Peltier (2000). "Subcontinental mantle dynamics : A further analysis based on the joint constraints of dynamic surface topography and free-air graviy". In: Journal of Geophysical Research 105(B3), pp. 5635–5662.

Parker, R. L. and D. W. Oldenburg (1973). "Thermal Model of Ocean Ridges". In: Nature Physical Science 242, pp. 137–139. doi: 10.1038/physci242137a0.

Parsons, B. and S. Daly (1983). "The relationship between surface topography, gravity anomalies, and temperature structure of convection". In: Journal of Geophysical Research 88(B2), pp. 1129–1144. doi: 10.1029/JB088iB02p01129.

Parsons, B. and D. McKenzie (1978). "Mantle convection and the thermal structure of the plates". In: Journal of Geophysical Research 83(B9), pp. 4485–4496. doi: 10.1029/JB083iB09p04485.

Parsons, B and J. Sclater (1977). "An analysis of the variation of ocean floor bathymetry and heat flow with age". In: Journal of Geophysical Research 82, pp. 803–827.

Pekeris, C. L. (1935). "Thermal convection in the interior of the Earth". In: Mon. Not. R. Astron. Soc., Geophys. Suppl. 3, pp. 343–367. doi: 10.1111/j.1365-246X.1935.tb01742.x.

Pérez-Díaz, L. and G. Eagles (2014). "Constraining South Atlantic growth with seafloor spreading data". In: Tectonics 33, pp. 1848–1873. doi: 10.1002 /2014TC003644.Received.

Pérez-Díaz, L. and G. Eagles (2017) A new high resolution seafloor age grid for the South Atlantic. Geochemistry, Geophysics, Geosystems, 18(1), pp. 457-470. doi: 10.1002/2016GC006750

Poore, H. R., R. Samworth, N. J. White, S. M. Jones, and I. N. McCave (2006). Neogene overflow of Northern Component Water at the Greenland-Scotland Ridge. In: Geochem. Geophys. Geosyst., 7, Q06010, doi:10.1029/2005GC001085.

759 Renkin, M. L. and J. G. Sclater (1988). “Depth and age in the North Pacific”. In: Journal of
760 Geophysical Research 93(B4), pp. 2919–2935. doi: 10.1029/JB093iB04p02919.

761 Richards, M. A. and B. H. Hager (1984). “Geoid anomalies in a dynamic Earth”. In: Journal
762 of Geophysical Research: Solid Earth 89(B7), pp. 5987–6002. doi:
763 10.1029/JB089iB07p05987.

764 Sandwell, D.T., Müller, R.D., Smith, W.H., Garcia, E. and Francis, R., 2014. New global
765 marine gravity model from CryoSat-2 and Jason-1 reveals buried tectonic structure: Science,
766 346(6205), pp.65-67.
767 Schubert, G, C. Froidevaux, and D. A. Yuen (1976). “Oceanic lithosphere and astenosphere:
768 thermal and mechanical structure”. In: Journal of Geophysical Research 81(20), pp. 3525–
769 3540.

770 Schubert, G and D. Turcotte (1972). “One-dimensional model of shallow mantle convection”.
771 In: Plate Tectonics. American Geophysical Union:Washington DC. doi:
772 10.1002/9781118782149.ch30.

773 Schubert, G. et al. (1978). “Mantle circulation with partial shallow return flow: Effects on
774 stresses in oceanic plates and topography of the sea floor”. In: Journal of Geophysical
775 Research 83(B2), p. 745. doi: 10.1029/JB083iB02p00745.

776 Sclater, J. G., S. Hellinger, and C. Tapscott (1977). “Paleobathymetry of Atlantic Ocean from
777 theJurassic to Present”. In: Journal of Geology 85(5), pp. 509–552.

778 Sclater, J. G., L. Meinke, and C. Murphy (1985). “The depth of the ocean through the
779 Neogene”. In: Geological Society of America Memoir 163, pp. 1–19.

780 Smith, W. H.,and Sandwell, D.T. (1997). “Global Sea Floor Topography from Satellite
781 Altimetry and Ship Depth Soundings”. In: Science 277, pp. 1956–1962. doi:
782 10.1126/science.277. 5334.1956.

783 Stein, C. and S Stein (1992). “A model for the global variation in oceanic depth and heat flow
784 with lithospheric age”. In: Nature 359, pp. 123–129.

785 Stein, C. A. and S. Stein (1994). “Thermal Evolution of Oceanic Lithosphere”. In:
786 Geophysical Research Letters 21(8), pp. 709–712.

787 Steinberger, B., Sutherland, R., and R. J. O'connell (2004). “Prediction of Emperor-Hawaii
788 seamount locations from a revised model of global plate motion and mantle flow”. In: Nature,
789 430(6996), 167-173.

790 Steinberger, B. and R. Holme (2008). “Mantle flow models with core-mantle boundary
791 constraints and chemical heterogeneities in the lowermost mantle”. In: Journal of
792 Geophysical Research: Solid Earth 113(5), pp. 1–16. doi: 10.1029/2007JB005080.

Sykes, T. J. (1996). "A correction for sediment load upon the ocean floor: Uniform versus varying sediment density estimations—implications for isostatic correction". In: Marine Geology 133, pp. 35–49. doi: 10.1016/0025-3227(96)00016-3.

Torsvik, T. H. et al. (2008). "Global Plate Motion Frames : toward a unified model". In: Reviews of Geophysics 46, pp. 1–44. doi: 10.1029/2007RG000227.1.INTRODUCTION.

Turcotte, D. and E. Oxburgh (1967). "Finite amplitude convection cells and continental drift". In: Journal of Fluid Mechanics 28, pp. 29–42.

Van Avendonk, H.J., Davis, J.K., Harding, J.L. and L. A. Lawver (2017). Decrease in oceanic crustal thickness since the breakup of Pangaea. In: Nature Geoscience, 10(1), pp.58-61.

White, R. S., D. McKenzie, and R. K. O'Nions (1992). "Oceanic crustal thickness from seismic measurements and rare earth element inversions". In: Journal of Geophysical Research 97(B13), pp. 19683–19715. doi: 10.1029/92JB01749.

Whittaker, J., A. Goncharov, S. Williams, R. D. Müller, and G. Leitchenkov (2013), Global sediment thickness data set updated for the Australian-Antarctic Southern Ocean. In: Geochem. Geophys. Geosyst., 14, 3297–3305, doi:10.1002/ggge.20181.

Wright, J. D. and K. G. Miller (1996). Control of North Atlantic Deep Water circulation by the Greenland-Scotland Ridge. In: Paleoceanography, 11, 157-170.

Tables

Table 1 Comparison of Corrected Water Depth values derived from DSDP drill core data with those obtained following the method described in this paper and those of Sykes *et al*., 1998.

Site	Age (Ma)	Lon	Lat	CWD[1]	CWD[2]	CWD[3]	Diff[a]	Diff[b]
361	129	15.45	-35.07	-5101	-5597	-5150	496	49
513	36	-24.64	-47.58	-4536	-4845	-5158	309	622
516	108	-35.28	-30.28	-1839	-1411	-1944	428	105
698	118	-33.1	-51.46	-2228	-3875	-2755	1647	527
701	53	-23.21	-51.98	-4842	-4935	-4868	93	26
703	92	7.89	-47.05	-1952	-3189	-2202	1237	250

[*] [1]Corrected Water Depth in drill core data (DSDP); [2]CWD (Sykes *et al*., 1998); [3]CWD (this study)
[†][a]CDW^1-CDW^2; [b]CDW^1 – CDW^3

Table 2 Summary of errors considered for the uncertainty analysis

	Source and nature of error						**Depiction of uncertainty**
	Oceanic Lithosphere age	*Onset of post-rift in COTZ*	*Sediment thickness*	*Crustal thickness*	*Dynamic topography*	*Height of LIP or aseismic ridge*	
Error that makes presented surface too deep	Too old	Negligible[1]	Too thin	Too thin	Too negative / not positive enough	Negligible[3]	Add summed errors to generate shallowest paleobathymetry for uncertainty
Error that makes presented surface too shallow	Too young	Too young	Negligible[2]	Too thick	Too positive / not negative enough	Too high for time slice	Subtract summed errors to generate deepest paleobathymetry for uncertainty

1. Ages assigned on basis of the oldest constrained oceanic age (Pérez-Díaz and Eagles, 2017), therefore youngest estimate. Older post-rift onsets therefore unreasonable.
2. Laske et al. (2013), and Whittaker et al. (2013) state that their sediment thicknesses are minimum estimates, as the base of the sediment pile may not be interpretable in some seismic data, or the reflection interpreted as from crystalline basement may be not be from basement rocks.
3. We consider it unlikely that LIPs lost considerable elevation over their lifetime. This is reasonable for submarine LIPs where erosion can be considered negligible.

Figure captions

Fig. 1. General tectono-structural map of the South Atlantic. AB: Argentine Basin; Afr: African Plate; AgB: Agulhas Basin; AnG: Angola Basin; Ant: Antarctic Plate; AP: Agulhas Plateau; BHp: Bouvet Hotspot; Cameroon VL: Cameroon Volcanic Line; DSm: Discovery Seamounts; HHp: St. Helena Hotspot; IOR: Islas Orcadas Rise; MR: Meteor Rise; NGR: North Georgian Rise; SAm: South American Plate; SHp: Shona Hotspot; ShR; Shona Ridge; SLR: Sierra Leona Rise; THp: Tristán da Cunha Hotspot.

Fig. 2. Depth-age data for the South Atlantic plotted over various thermal model curves. Age data: seafloor age grid of Pérez Díaz & Eagles (2017). Depth data: extracted from a bathymetric map of the South Atlantic corrected for sedimentation, crustal thickness variations and dynamic topography. Red circles and black bars are averages and standard deviations calculated for each 5 My bin. GDH1: Stein and Stein (1994); CHABLIS: Doin and Fleitout (1996); Xby: Crosby and McKenzie (2006); PSM: Parsons and Sclater (1977); HW: Hillier and Watts (2005) and HSM: Davis and Lister (1974).

Fig. 3. For 70 Ma, (**a**) Palaeoage grid and (**b**) seafloor depths as predicted by GDH1 (Stein & Stein 1992).

Fig. 4. (**a**) COTZ extent along the margins of the South Atlantic. COB ensembles are those compiled by Eagles *et al.* (2015). (**b**) and (**c**) COTZ cross-sections. Dashed lines: depths extracted from a corrected present day bathymetry map. Solid lines: depths corrected to account for depth of IL as predicted by GDH1 at time *t*. Magenta lines: edge-of-plate flexural curve. Green lines: intraplate flexural curve.

Fig. 5. Predicted basement depths at (**a**) present day and (**b**) 70 Ma.

Fig. 6. Residual bathymetry anomalies at present day (*R*).

Fig. 7. (**a**) Sediment thickness map of Laske et al. (2013), (**b**) Modelled depths modified to include the effects of variable sediment thickness and (**c**) R_s; Residual bathymetry anomalies remaining after applying the sediment correction.

Fig. 8. (**a**) Crystalline crustal thickness estimates of CRUST1.0 (Laske et al., 2013), (**b**) Modelled basement depths modified to account for variable sediment and crustal thickness and (**c**) R_{sc}; Residual bathymetry anomalies remaining after applying the sediment and crustal thickness corrections.

Fig. 9. (**a**) Dynamic topography at present day (Müller et al., 2008b), (**b**) Modelled basement depths after incorporating the effects of loading, stretching and dynamic topography and (**c**) R_{scd}; Residual bathymetry anomalies remaining after accounting for sediment and crustal thickness variations and dynamic topography.

Fig. 10. (**a**) Sediment thickness map of Laske *et al.*(2013) (**b**) Sediment thickness as predicted from residual bathymetry anomalies (R_{cd}). S2 is an area of thick sediment within the Argentine Basin mentioned in text.

Fig. 11. (**a**) Crustal thickness map of CRUST1.0 (Laske et al., 2013). (**b**) Crustal thickness as predicted from residual bathymetry anomalies (R_{sd}). C1 and C2: see text for details.

Fig. 12. (**a**) Dataset of dated samples along hotspot tracks in the South Atlantic (O'Connor and Duncan, 1990; O'Connor et al., 2012; O'Connor and Jokat, 2015). Background shows R_{scd}. (**b**) Modelled basement depths as in fig. 8b, modified to account for the topography of aseismic ridges. (**c**) Residual bathymetry anomalies after subtracting (b) from present-day satellite-derived bathymetry.

Fig. 13. (**a**) Dynamic topography in the South Atlantic as modelled by Bernhard Steinberger (Müller *et al*. 2008b). (**b**) Dynamic topography as predicted from residual bathymetry anomalies (R_{sc}).

Fig. 14. Combined effects of all uncertainties that imply the modelled 60 Ma bathymetry might be (a) deeper or (b) shallower than a less uncertain model might show.

Fig. 15. (a) Satellite altimetry derived present day bathymetry, (b) Present day bathymetry modelled following the workflow presented on this paper and (c) Significant (>50 km diameter) areas in which measured present-day bathymetry lies deeper than its deepest modelled equivalent within uncertainty (blues) or shallower than its shallowest modelled equivalent within uncertainty.

Fig. 16. (a) Paleobathymetric reconstruction at 60 Ma, with (b) minimum and (c) maximum depth uncertainty estimates in inset.

888 **Figure 1**

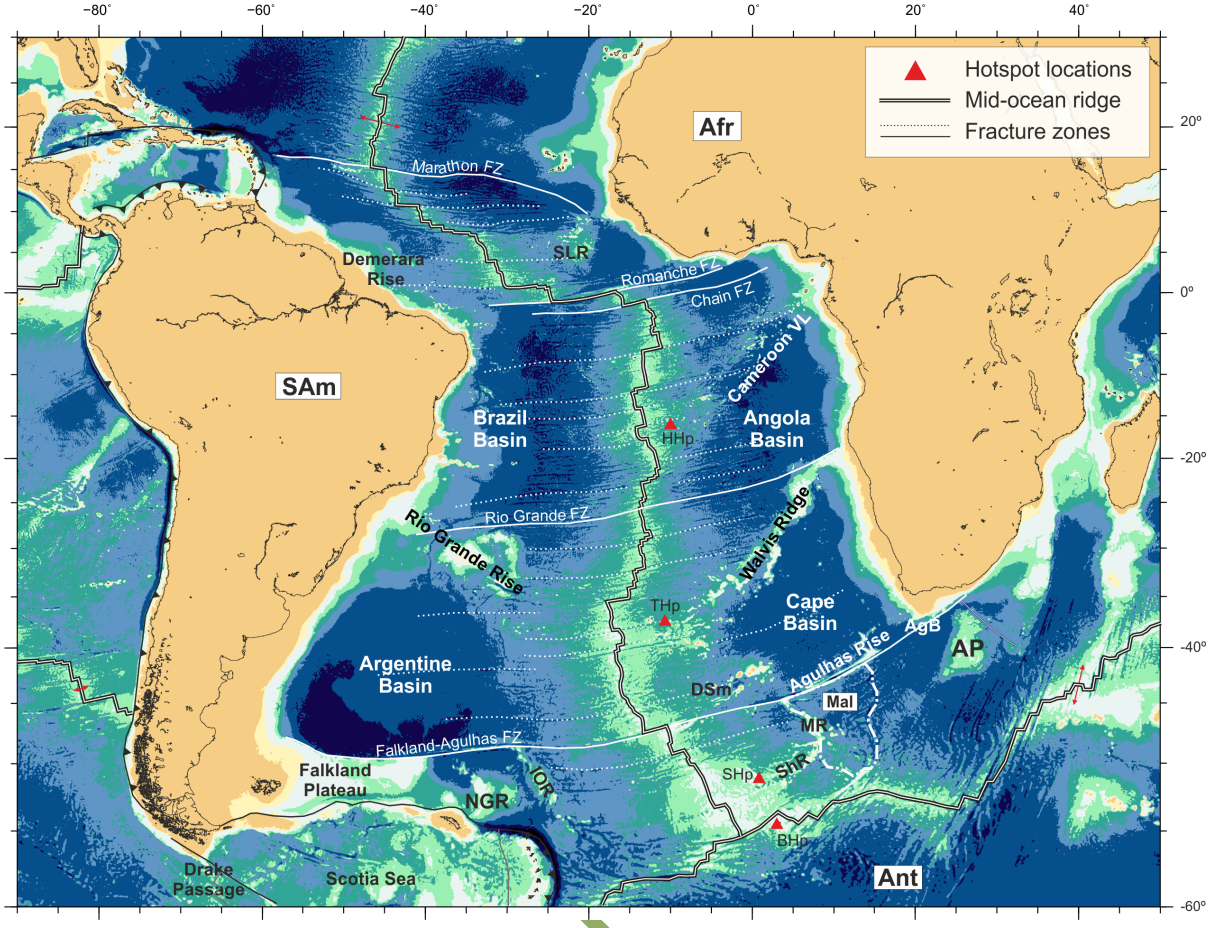

889

890

891

892 **Figure 2**

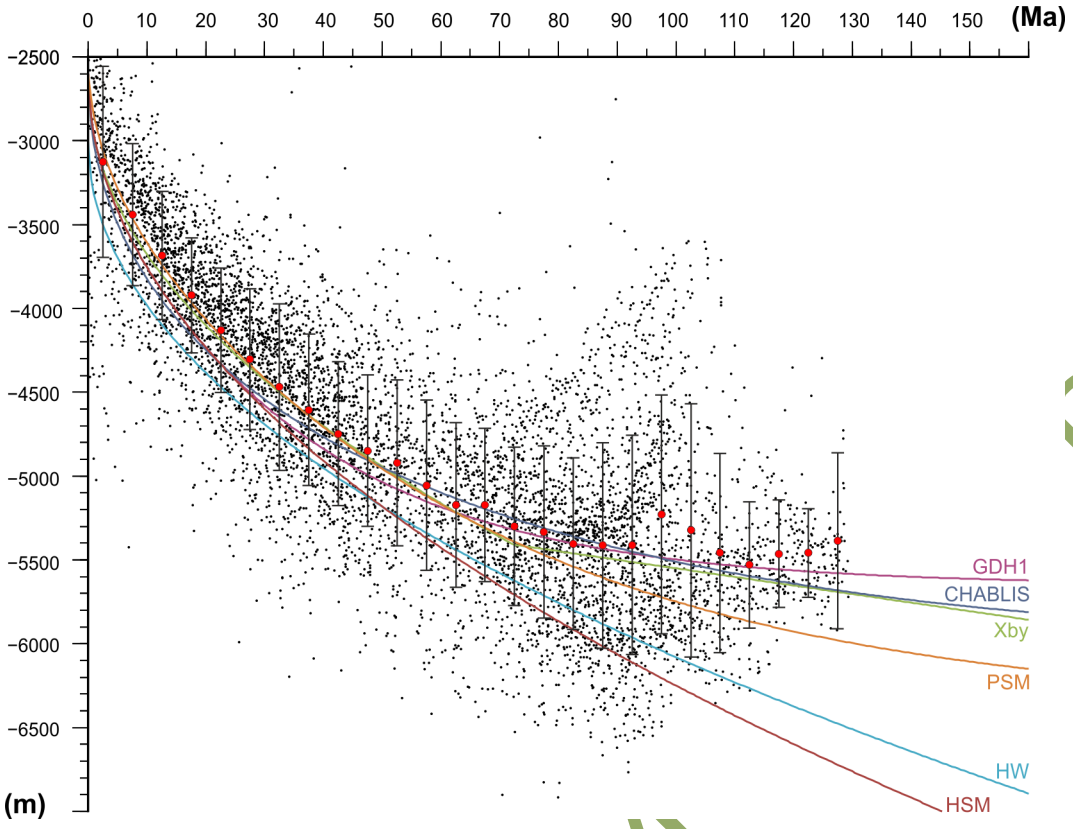

893

894

Figure 3

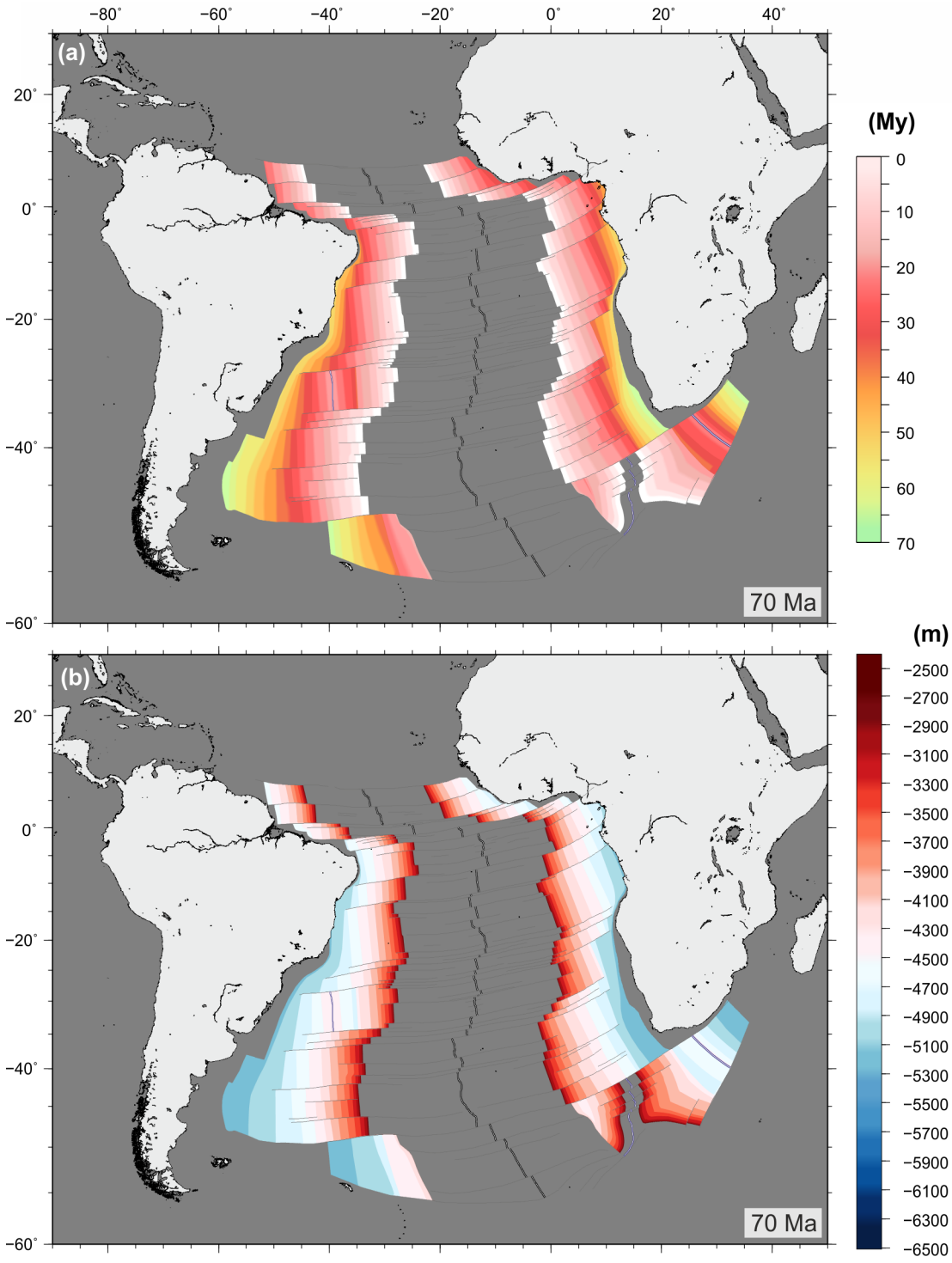
(a)
70 Ma
(b)
70 Ma
(My)
0
10
20
30
40
50
60
70
(m)
−2500
−2700
−2900
−3100
−3300
−3500
−3700
−3900
−4100
−4300
−4500
−4700
−4900
−5100
−5300
−5500
−5700
−5900
−6100
−6300
−6500
−80°
−60°
−40°
−20°
0°
20°
40°
20°
0°
−20°
−40°
−60°

899 **Figure 4**

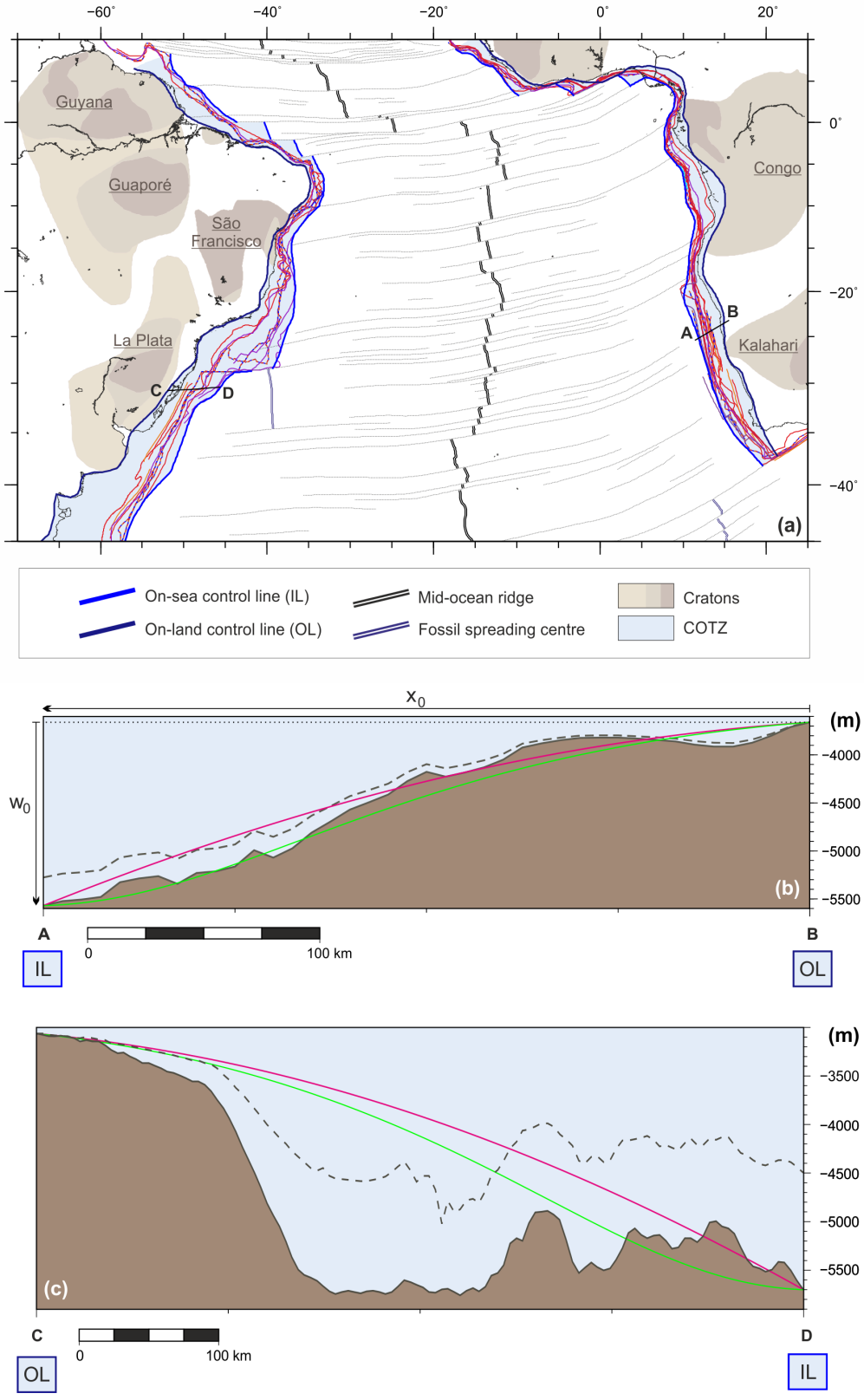

900

901

902

903 **Figure 5**

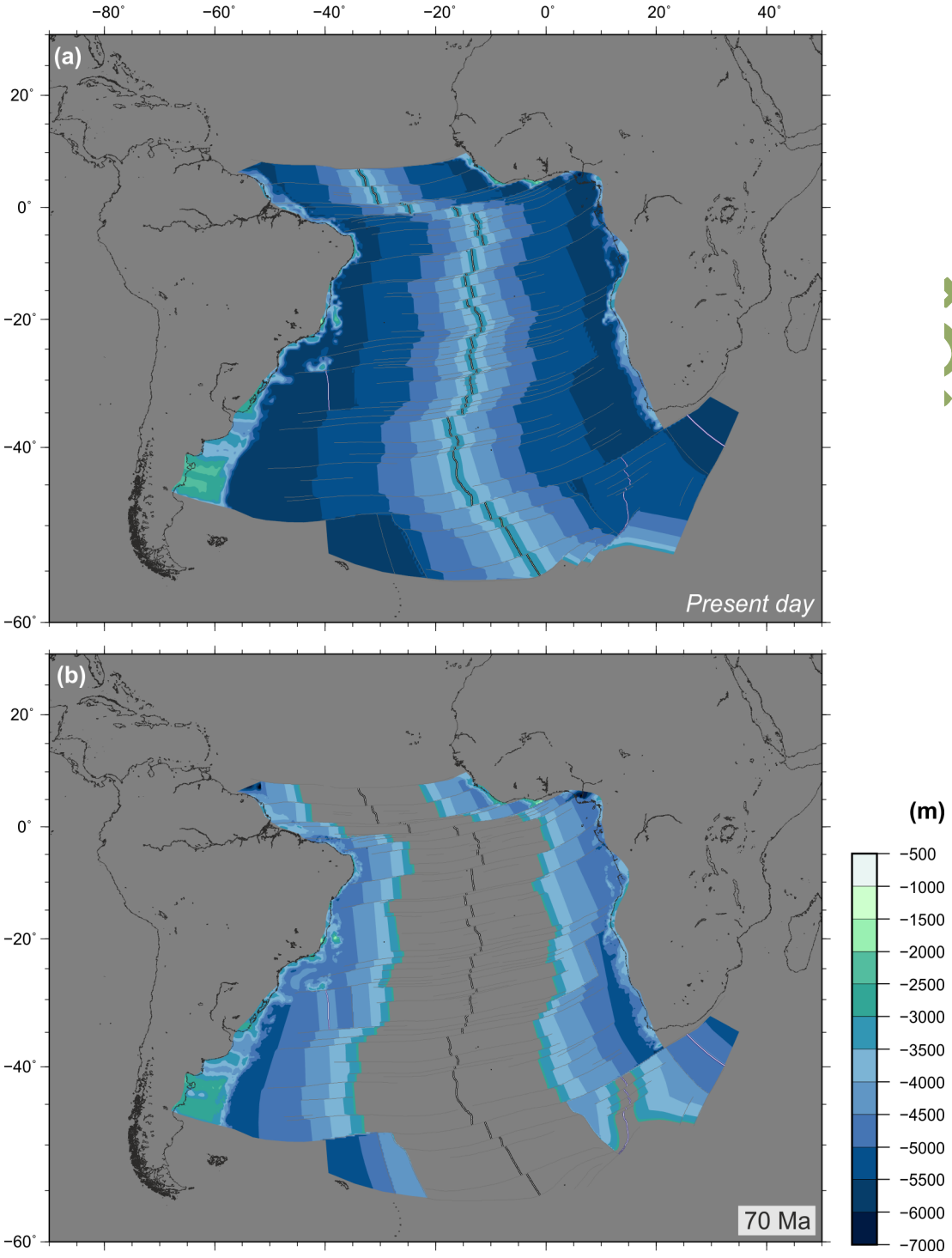

904

905

906

907 **Figure 6**

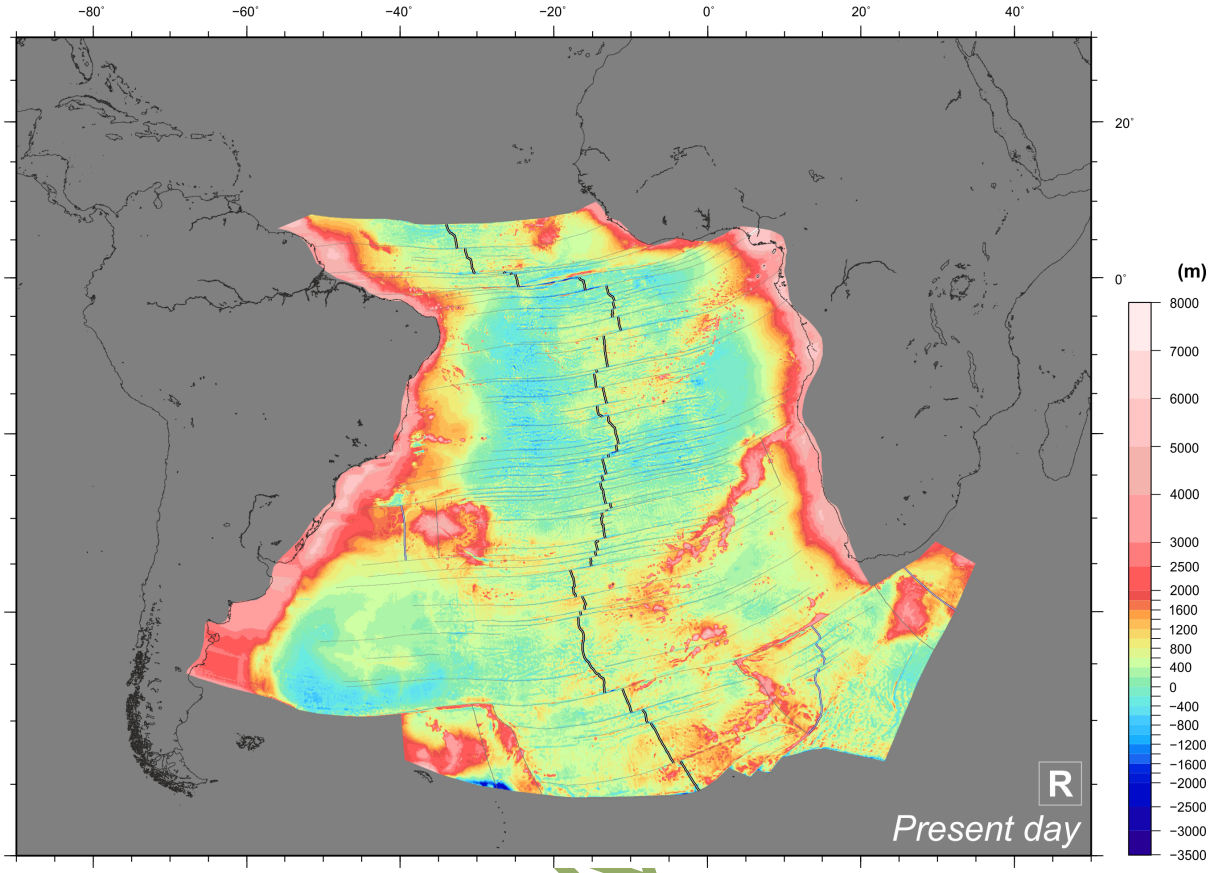

908

909

910

911 **Figure 7**

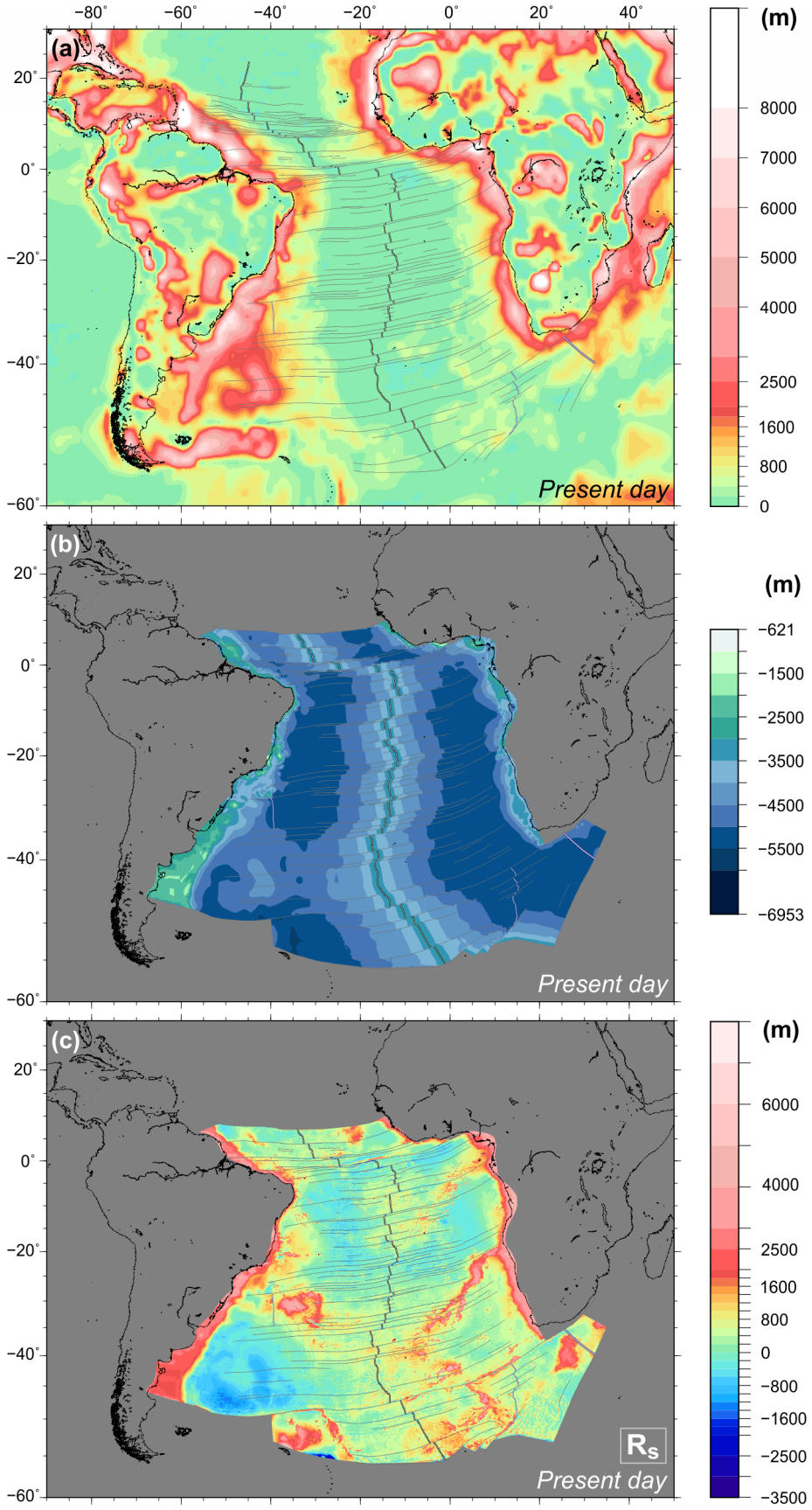

912

913

914 **Figure 8**

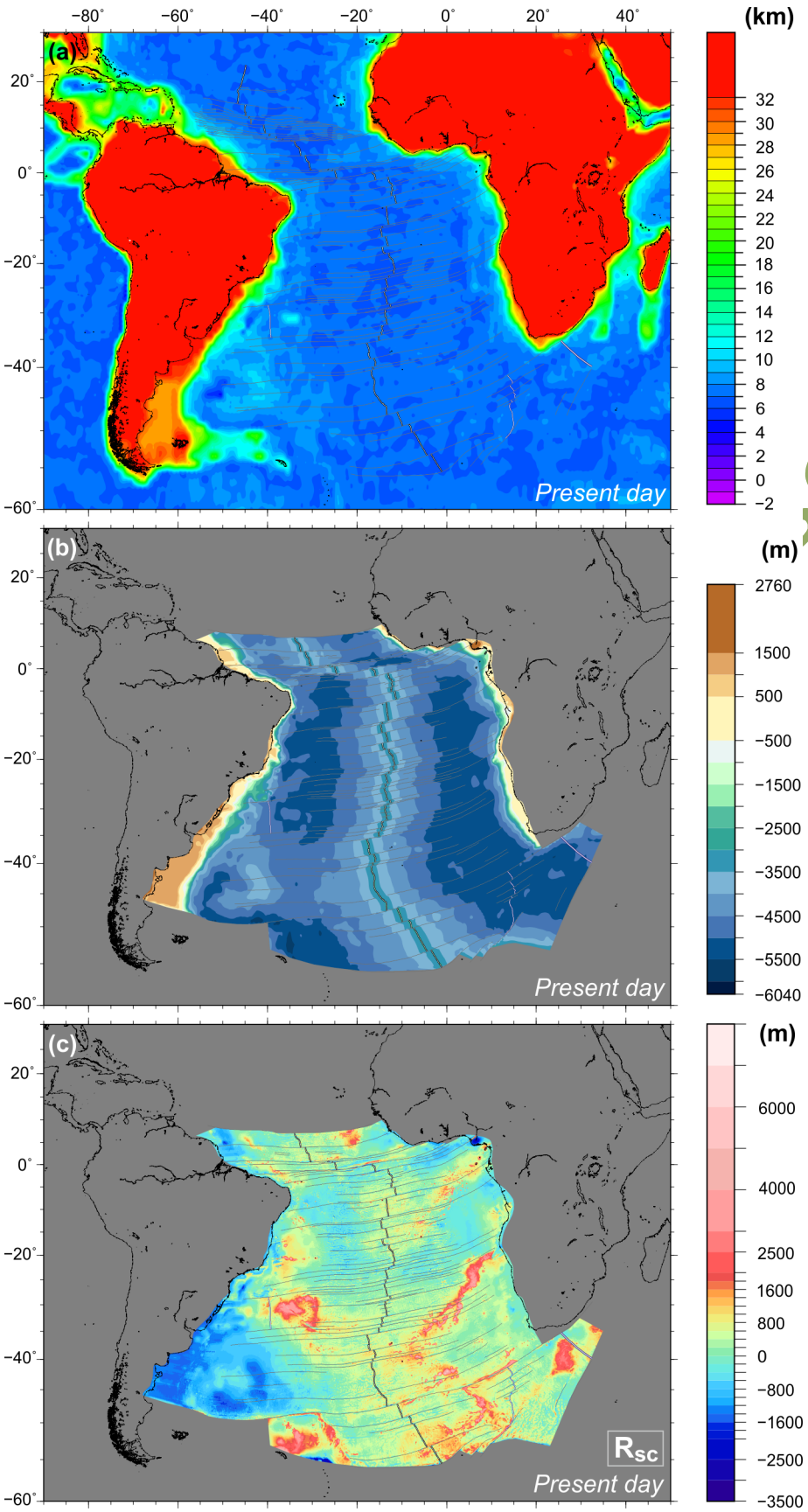

915

916 **Figure 9**

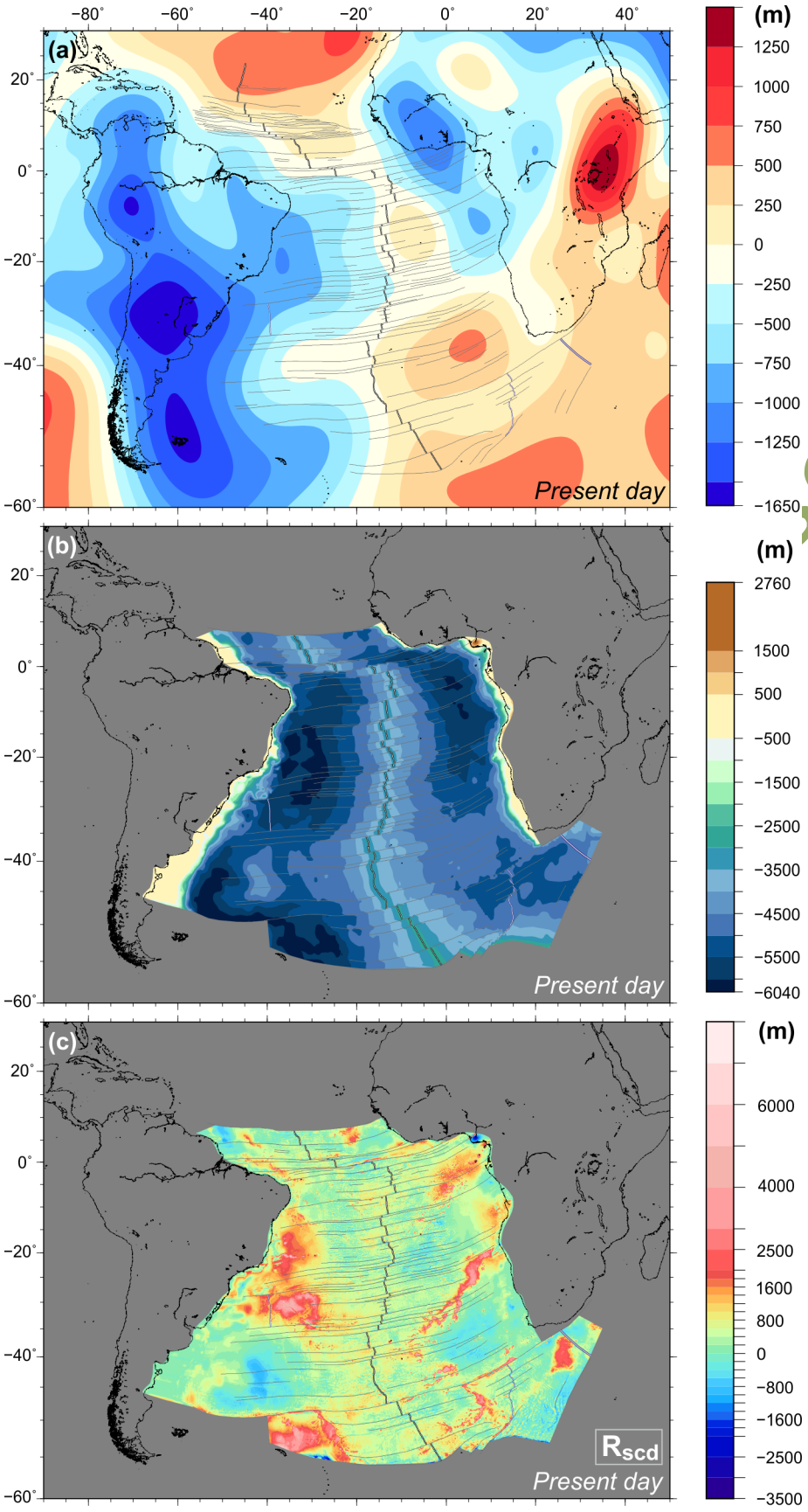

917

Figure 10

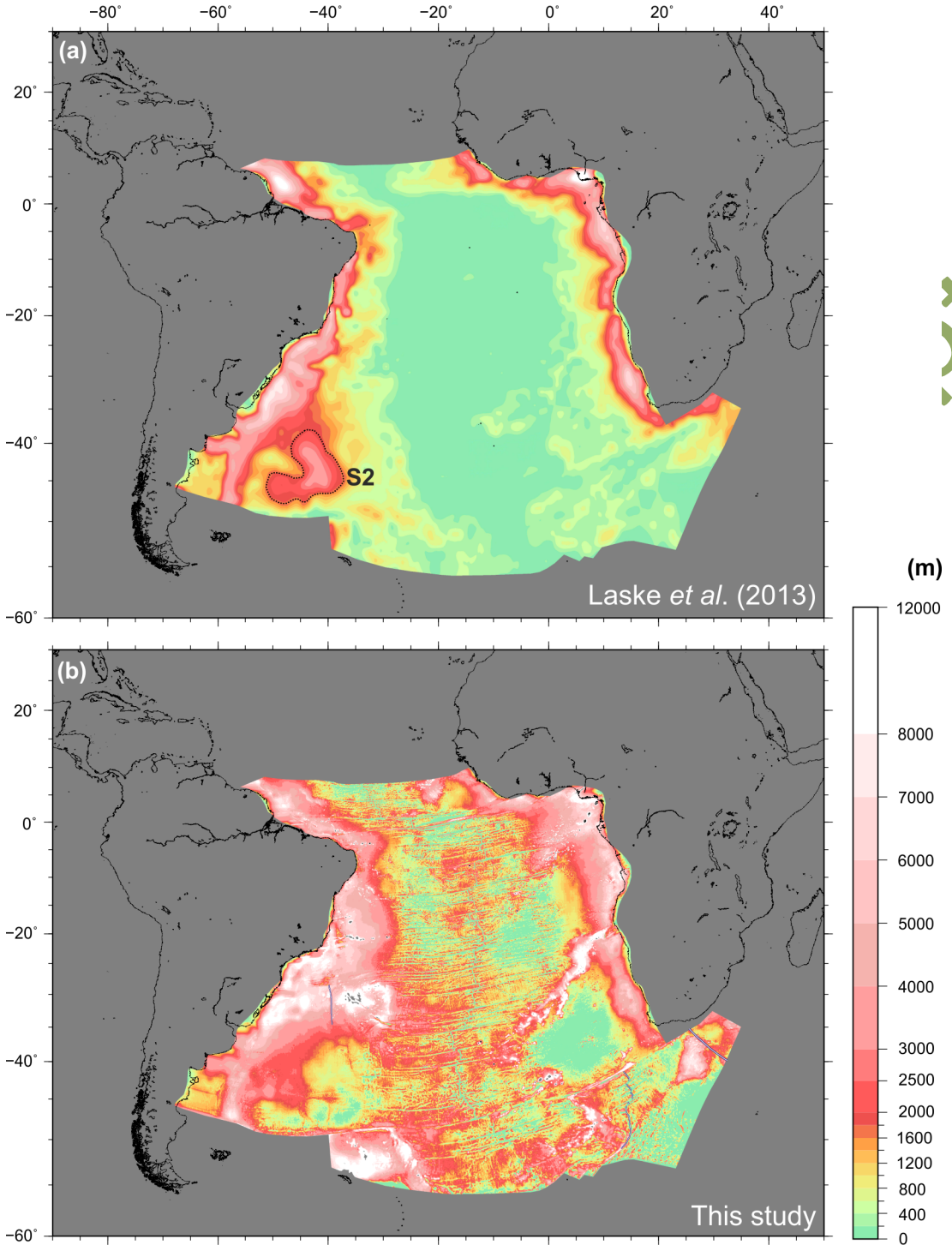
(a)
S2
Laske et al. (2013)
(b)
This study
(m)
12000
8000
7000
6000
5000
4000
3000
2500
2000
1600
1200
800
400
0
−80°
−60°
−40°
−20°
0°
20°
40°
20°
0°
−20°
−40°
−60°

922 **Figure 11**

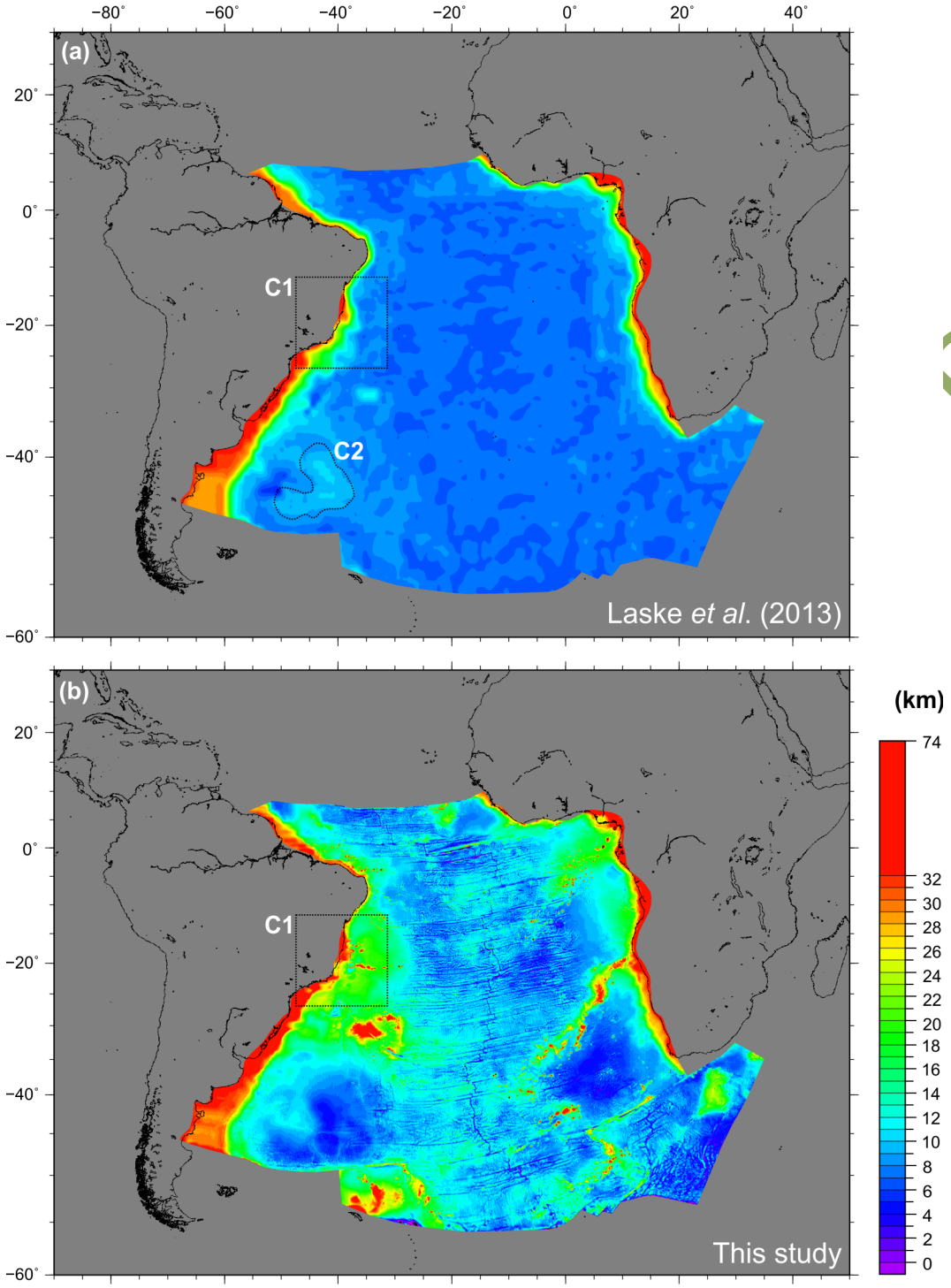

923

924

925

926 **Figure 12**

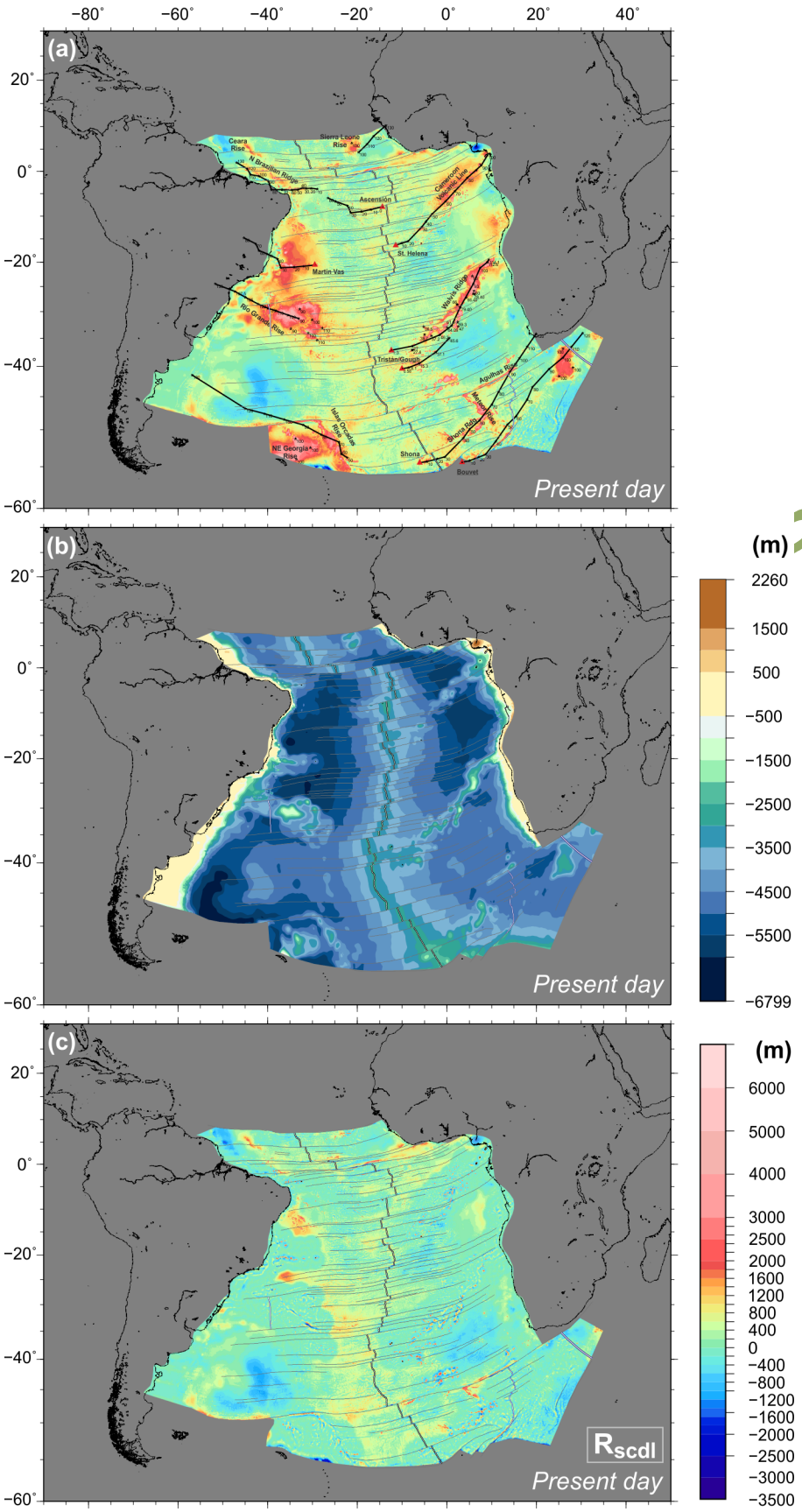

927

928

Figure 13

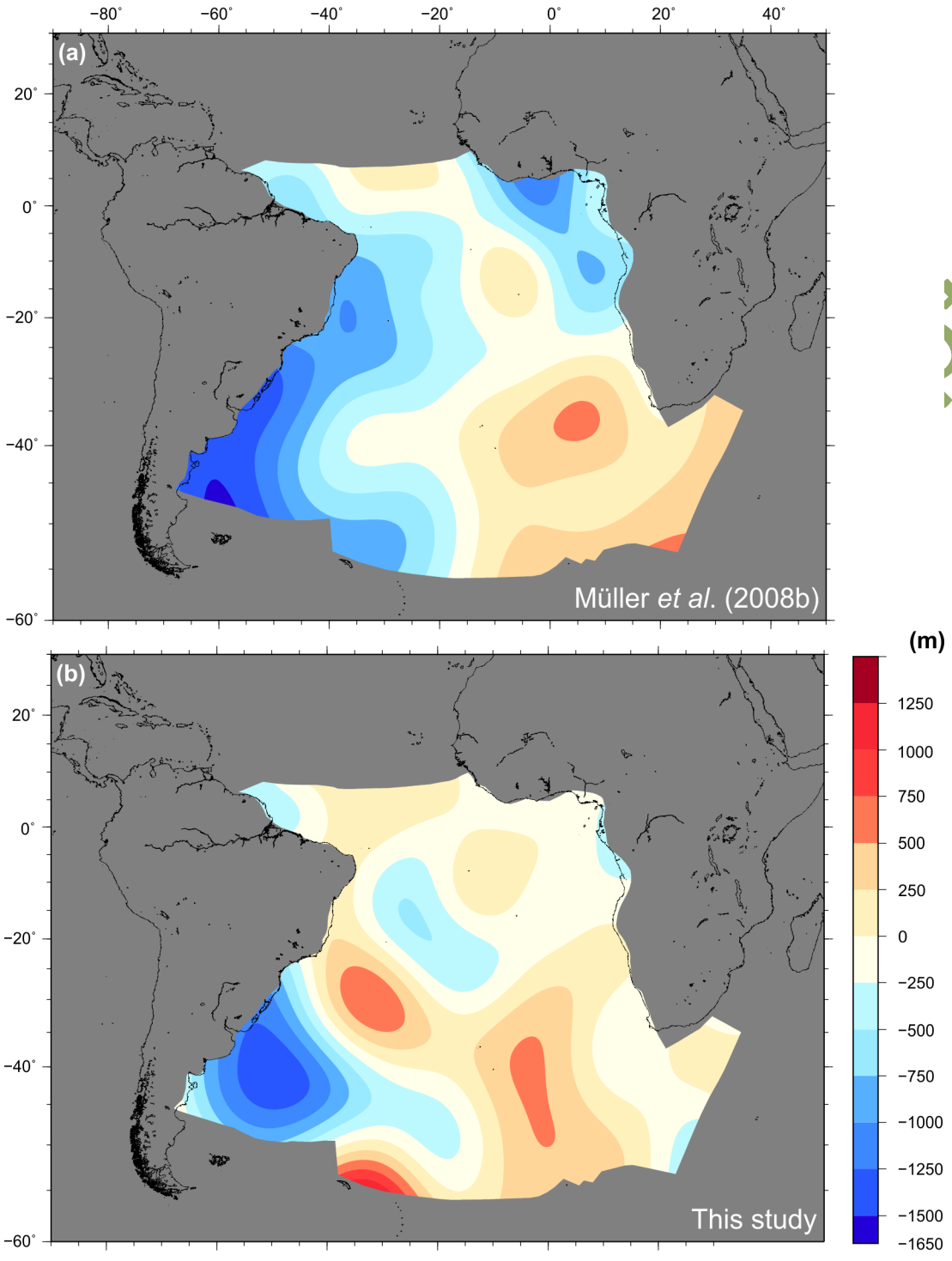
(a)
(b)
Müller et al. (2008b)
This study
−80°
−60°
−40°
−20°
0°
20°
40°
20°
0°
−20°
−40°
−60°
(m)
1250
1000
750
500
250
0
−250
−500
−750
−1000
−1250
−1500
−1650

933 **Figure 14**

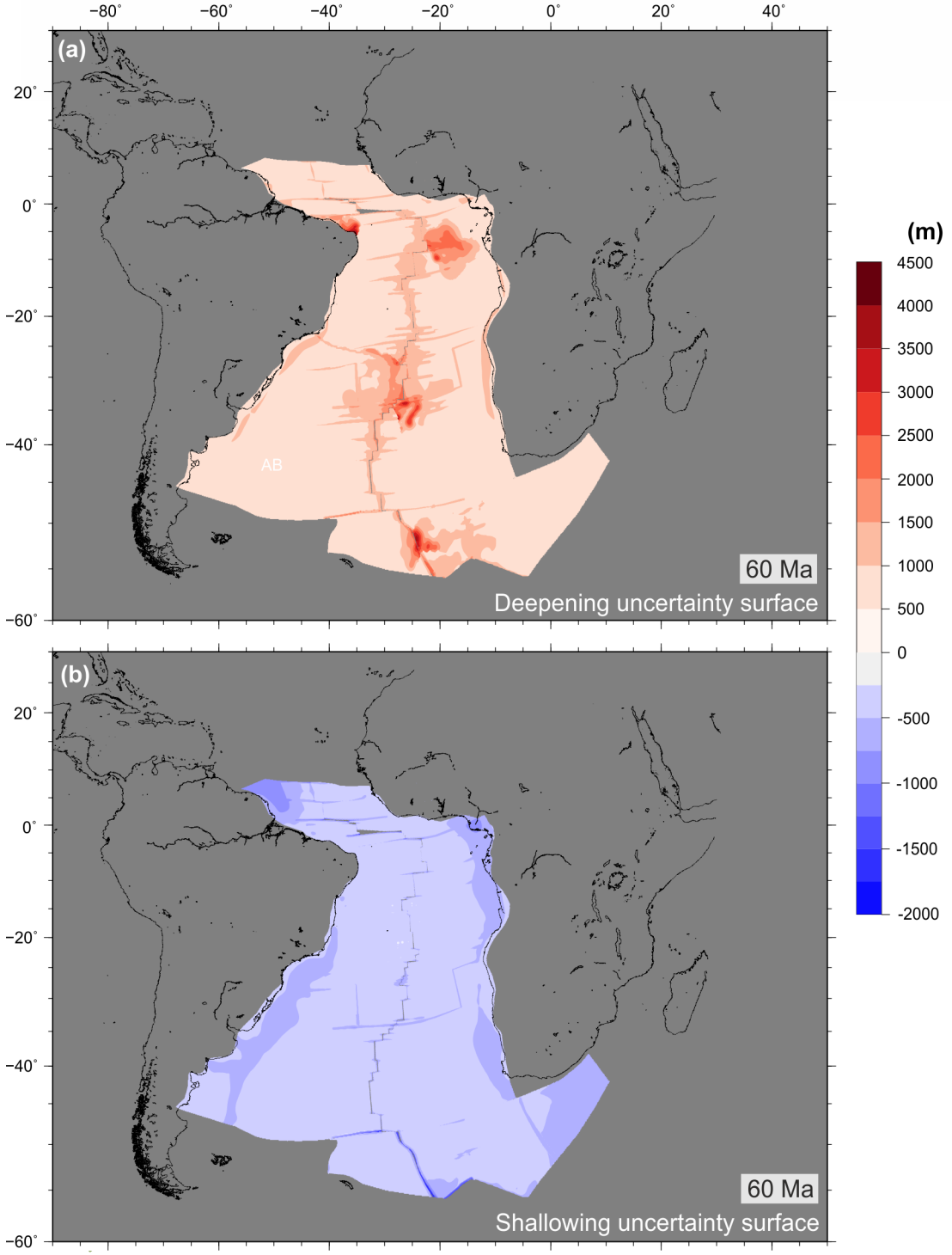

934

935

936

937

938 **Figure 15**

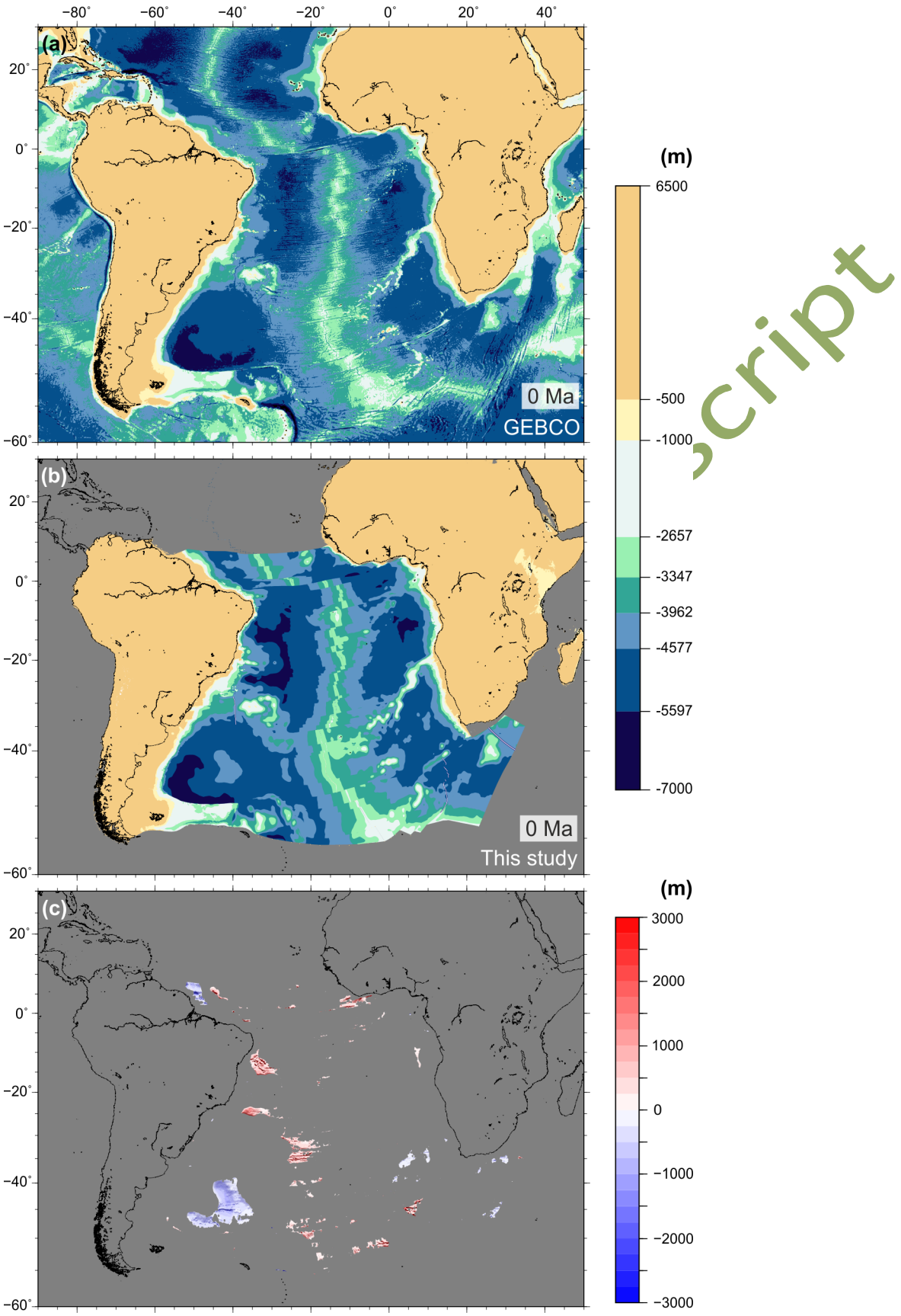

946

947

948 **Figure 16**

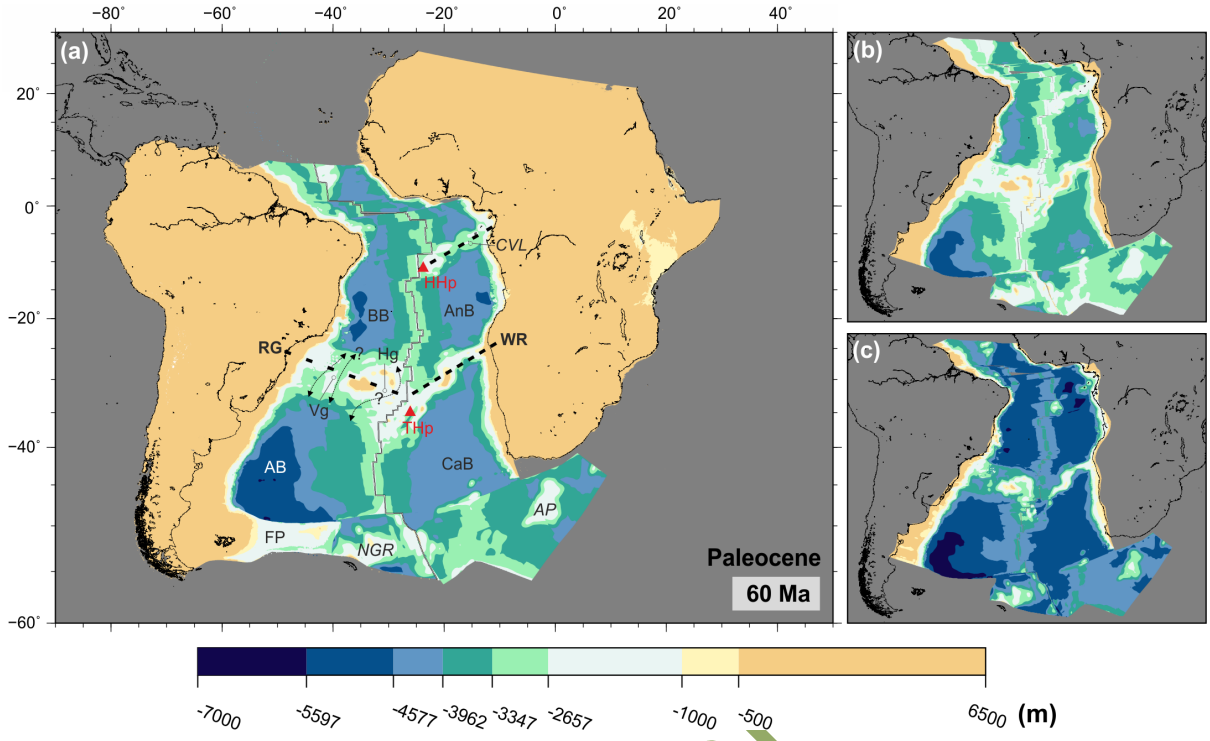

949

950

951